

1 **Revision 2**

2 **Wenlanzhangite–(Y) from the Yushui deposit, South China: a potential proxy for**  
3 **tracing the redox state of ore formation**

4 Peng Liu<sup>1\*</sup>, Guowu Li<sup>2</sup>, Ningyue Sun<sup>2</sup>, Wei Yao<sup>1,3</sup>, Hong Yu<sup>4</sup>, Yongfei Tian<sup>2</sup>, Wenqiang Yang<sup>1</sup>,  
5 Fengshang Zhao<sup>1</sup>, Nigel J. Cook<sup>5</sup>

6 <sup>1</sup> State Key Laboratory of Continental Dynamics, Department of Geology, Northwest University,  
7 Xi'an 710069, China

8 <sup>2</sup> Crystal Structure Laboratory, Science Research Institute, China University of Geosciences, 100083  
9 Beijing, China

10 <sup>3</sup> Xi'an Center of Mineral Resources Survey, China Geological Survey, Xi'an 710100, China

11 <sup>4</sup> Ministry of Natural Resources (MNR) Key Laboratory of Metallogeny and Mineral Assessment,  
12 Institute of Mineral Resources, Chinese Academy of Geological Sciences (CAGS), Beijing 100037,  
13 China

14 <sup>5</sup> School of Chemical Engineering, The University of Adelaide, Adelaide, South Australia 5005,  
15 Australia

16 **Corresponding author:** Peng Liu, [pengliu@nwu.edu.cn](mailto:pengliu@nwu.edu.cn)

## ABSTRACT

23  
24 Mineral phases in which vanadium (V) and heavy-rare-earth elements (HREEs) coexist are rarely  
25 documented. Here, we report a new V-HREE-bearing silicate mineral species, wenlanzhangite-(Y),  
26 which is a vanadiferous derivate of jingwenite-(Y)  $[Y_2Al_2V^{4+}_2(SiO_4)_2O_4(OH)_4]$  coexisting with  
27 jingwenite-(Y) in bedded/massive ores at Yushui, South China. Wenlanzhangite-(Y) forms as a dark  
28 brown, 70–100  $\mu\text{m}$ -thick rim on a core domain of jingwenite-(Y), which occurs as 100–200  $\mu\text{m}$   
29 columnar crystals. The colour, streak, lustre, and hardness (Mohs) are dark brown, yellow grey,  
30 vitreous, and  $\sim 4$ , respectively. Compared to jingwenite-(Y), wenlanzhangite-(Y) has higher  
31 vanadium and lower aluminium contents. Calculated on the basis of 8 cations, the empirical formula  
32 is

33  $(Y_{1.26}Dy_{0.17}Er_{0.11}Gd_{0.09}Yb_{0.09}Nd_{0.09}Sm_{0.06}Sc_{0.04}Ho_{0.03}Ce_{0.02}Tb_{0.02}Tm_{0.02}Pr_{0.01})_{\Sigma 2.00}(V^{3+}_{1.46}Al_{0.54})_{\Sigma 2.00}V^{4+}$   
34  $_2(SiO_4)_2O_4(OH)_4$ , which can be simplified to the ideal formula  $Y_2V^{3+}_2V^{4+}_2(SiO_4)_2O_4(OH)_4$ .

35 Wenlanzhangite-(Y) is triclinic, with space group  $P-1(\#2)$ ,  $Z = 2$ , and unit-cell parameters  $a =$   
36  $5.9632(7) \text{ \AA}$ ,  $b = 9.599(1) \text{ \AA}$ ,  $c = 9.9170(9) \text{ \AA}$ ,  $\alpha = 90.033(8)^\circ$ ,  $\beta = 98.595(2)^\circ$ ,  $\gamma = 90.003(9)^\circ$ , and  $V$   
37  $= 561.28(10) \text{ \AA}^3$ . Wenlanzhangite-(Y) is approved by the International Mineralogical Association  
38 Commission on New Minerals, Nomenclature and Classification (IMA2022–142). The structure of  
39 wenlanzhangite-(Y) is composed of  $a$ -axis-oriented chains of  $[VO_6]$  octahedra consisting of edge-  
40 sharing octahedra linked by insular  $[SiO_4]$  tetrahedra, leaving open channels occupied by rare earth  
41 elements. Observed compositional variation and crystal structure demonstrate that  $V^{3+}$  can substitute  
42 for  $Al^{3+}$  in jingwenite-(Y), forming wenlanzhangite-(Y). The occurrence of wenlanzhangite-(Y)  
43 indicates a relatively more reducing hydrothermal environment causing reduction of  $V^{5+}$  in oxidized  
44 fluids to  $V^{3+}$  and thus represents a useful proxy for tracing the redox state of ore formation.

45 **Keywords:** New mineral; Wenlanzhangite–(Y); Heavy rare earth elements; Yushui Cu deposit

## INTRODUCTION

Recent studies have reported the first account of significant HREE (and associated U) mineralization within a sediment-hosted Cu deposit, the Yushui deposit, South China (Liu et al. 2023). It is well known that sandstone-hosted uranium deposits can host economic concentrations of V (e.g., Colorado Plateau, USA) (Dahlkamp 2010), and form at an oxidation-reduction interface (Northrop et al. 1990; Shawe 2011). Vanadium, as  $V^{3+}$ ,  $V^{4+}$ ,  $V^{5+}$ , or a combination thereof, can occur as oxide phases or is combined with redox-sensitive elements (Weeks et al. 1959). In practice, V-HREE-bearing mineral phases are rarely documented.

A new V-HREE-bearing silicate mineral, jingwenite-(Y) [ $Y_2Al_2V^{4+}_2(SiO_4)_2O_4(OH)_4$ ], has been discovered and is an abundant phase in the Yushui deposit (Liu et al. 2023). Here we describe a vanadiferous derivate of jingwenite-(Y) from Yushui, wenlanzhangite-(Y), ideally  $Y_2V^{3+}_2V^{4+}_2(SiO_4)_2O_4(OH)_4$ . Wenlanzhangite-(Y) has been approved by the International Mineralogical Association Commission on New Minerals, Nomenclature and Classification (IMA2022-142). It is named in honor of Professor Wenlan Zhang (born in 1957), a famous expert in electron probe microbeam analysis at the School of Earth Sciences and Engineering, Nanjing University, China. She has published more than 80 papers that contribute to improvements and capabilities of electron probe analysis technology in China. Type material is deposited in the mineralogical collections of the Geological Museum of China, catalogue number GMCTM 2202.

## GEOLOGICAL BACKGROUND

The Yushui deposit, located in the southwestern domain of the southeastern coastal belt, South China (Fig. 1a), is a small yet high-grade Cu deposit with significant HREE enrichment, and minor enrichment in U, Co, and V (Liu et al. 2023). Mineralization is concealed beneath Late-Jurassic volcanic cover and is hosted at the unconformity between Upper Carboniferous dark grey dolostone/limestone with organic- and apatite-rich beds and a >300 m-thick sequence of Lower Carboniferous red sandstone (Figs. 1, 2a, and 2b) characterized by an abundance of heavy minerals

71 including clastic xenotime-(Y), rutile, zircon, and hematite. There are three types of Cu ore: I)  
72 bedded/massive; II) disseminated; and III) vein-type (Fig. 2c–g). HREE-bearing minerals occur  
73 mainly in bedded/massive ore (orebody V<sub>1</sub>). Based on mineral assemblages, orebody V<sub>1</sub> can be split  
74 into: I) a lower chalcopyrite-rich part; and II) an upper galena-rich part. The lower part is  
75 characterized by chalcopyrite, and abundant HREE-V- and V-Sc-bearing minerals including  
76 nolanite, thortveitite, roscoelite, xenotime-(Y), jingwenite-(Y) (Liu et al. 2023), hingganite-(Y),  
77 bastnäsite-(Y) and an unknown V-HREE-Sc-bearing silicate mineral phase. Minor components  
78 include bornite, barite, sphalerite, galena, uraninite, and quartz. The upper part of the orebody  
79 underlies the dolostone, and is dominated by galena, sphalerite, bornite, chalcopyrite, and hematite,  
80 and minor anhydrite, calcite, and apatite. Wenlanzhangite-(Y) occurs in the lower part of the  
81 bedded/massive orebody, and associated minerals are chalcopyrite, bornite, nolanite, thortveitite,  
82 jingwenite-(Y), and roscoelite (Fig. 3a). Wenlanzhangite-(Y) is observed as a dark brown, 70–100  
83 μm-thick rim on a core domain of jingwenite-(Y) or 100 μm-thick core on jingwenite-(Y), which  
84 occurs as 100–200 μm columnar crystals (Fig. 3b–d). The crystals display regular oscillatory  
85 compositional zoning on back-scattered electron images (Fig. 3b).

## 86 ANALYTICAL METHODS

### 87 Reflectance measurements

88 Reflectance values for wenlanzhangite-(Y) were measured in air using a CRAIC 20/30PV Pro  
89 microspectrophotometer at Westlake University, Hangzhou, China. The reference material is  
90 aluminum metal (R= 85-90 %) (SPFS) with MgF<sub>2</sub> coating. Reflectance values were obtained from  
91 five spots in a single wenlanzhangite-(Y) grain, with × 50 objective and 16 × 16 μm aperture size.

### 92 Chemical composition analysis

93 Quantitative major-element analysis was performed at Xi'an Center of Mineral Resources Survey,  
94 China, using a Shimadzu EPMA-1720HT electron microprobe. All measurements were performed

95 using an accelerating voltage of 15 kV and a beam current of 50 nA. The beam size was 20  $\mu\text{m}$  for  
96 the standards and 5  $\mu\text{m}$  for wenlanzhangite-(Y). Crystals used were PET (Y, Sc and Si), LIF (Ce, Pr,  
97 Nd, Sm, Gd, Tb, Dy, Ho, Er, Tm, Yb and V), and RAP (Al). The  $K\alpha$  line was chosen for analysis of  
98 Si, Al, V, and Sc; the  $L\alpha$  line for Ce, Pr, Sm, Nd, Tb, Gd, Dy, Er, Yb, and Y; and the  $L\beta$  line for Ho  
99 and Tm. Count times on peaks were 10 s and background intensities were measured on both sides of  
100 the peak for half of the peak time. The standards were  $\text{CeP}_5\text{O}_{14}$  for Ce,  $\text{PrP}_5\text{O}_{14}$  for Pr,  $\text{NdP}_5\text{O}_{14}$  for  
101 Nd,  $\text{SmP}_5\text{O}_{14}$  for Sm,  $\text{GdP}_5\text{O}_{14}$  for Gd,  $\text{Tb}_3\text{Ga}_5\text{O}_{12}$  for Tb,  $\text{DyP}_5\text{O}_{14}$  for Dy,  $\text{HoP}_5\text{O}_{14}$  for Ho,  $\text{ErP}_5\text{O}_{14}$   
102 for Er,  $\text{TmP}_5\text{O}_{14}$  for Tm,  $\text{YbP}_5\text{O}_{14}$  for Yb,  $\text{Y}_2\text{SiO}_5$  for Y and Si, kyanite for Al,  $\text{YVO}_4$  for V and pure  
103 Sc for Sc. Element mapping was carried out using a JEOL JXA-8230 electron microprobe at the  
104 State Key Laboratory of Continental Dynamics, Northwest University (China), with an accelerating  
105 voltage of 15 kV, beam current of 50 nA and beam diameter of 2  $\mu\text{m}$ .

106 In-situ trace element analysis was undertaken at the State Key Laboratory of Continental  
107 Dynamics, Northwest University (China). An Agilent 7900 ICP-MS coupled with RESolution M-50  
108 193-nm ArF Excimer Laser Ablation system was used to analyze mineral chemical compositions on  
109 polished thin sections. He and Ar were mixed via a T-connector before entering the ICP.  
110 International standard reference materials NIST SRM 610, NIST SRM 612, and BCR-2G were used  
111 as external standards for calculations (Bao et al. 2016). The concentration of Si obtained by EPMA  
112 was used as the internal standard for trace element content calculations. Data processing was  
113 performed using ICPMSDataCal (Liu et al. 2008).

#### 114 **Crystal structure analysis**

115 A transparent single crystal ( $0.02 \times 0.015 \times 0.01$  mm) was cut from the polished section on a double-  
116 focused ion beam platform (TESCAN GAIA 3). This crystal was used for the subsequent X-ray  
117 diffraction study. X-ray powder and single-crystal diffraction were carried out at the Science  
118 Research Institute, China University of Geosciences, China, with a Rigaku Oxford diffraction  
119 XtaLAB PRO-007HF single crystal diffractometer equipped with a rotating anode microfocus X-ray

120 source (50 kV, 24 mA; MoK $\alpha$ ,  $\lambda = 0.71073 \text{ \AA}$ ) and a hybrid pixel array detector. The crystal structure  
121 determination and refinement process of wenlanzhangite-(Y) were performed using OLEX2-1.3  
122 (Dolomanov et al. 2009). The structure model was solved with the SHELXT using intrinsic phasing  
123 and refined by SHELXL with least square (Sheldrick 2015a, b). Since the crystal cell parameters  
124 obtained by X-ray single crystal diffraction were close to a monoclinic cell and different from those  
125 of jingwenite-(Y), selected-area electron diffraction (SAED) analyses for wenlanzhangite-(Y) were  
126 undertaken to confirm the single crystal data. Experiments were performed using a JEM-2100 (HR)  
127 Transmission Electron Microscope equipped with a double-tilt holder, a Gatan digital camera, and an  
128 INCA Energy TEM100 energy-dispersive spectroscopy instrument at the Institute of Mineral  
129 Resources, Chinese Academy of Geological Sciences, Beijing, operated at 200 kV. A TEM foil of  
130 about 50 nm thickness was prepared on a FIB-SEM platform (TESCAN GAIA 3) at the analytical  
131 laboratory of the Beijing Research Institute of Uranium Geology. Images of the foil and its location  
132 in polished section before cutting are shown in Fig. 3b. Results were successfully indexed with  $P-1$   
133 model and the calculated parameters are listed below.

### 134 **Raman spectroscopy analysis**

135 Raman spectra of wenlanzhangite-(Y) were collected from a randomly oriented grain using a  
136 Renishaw Invia confocal Raman spectrometer equipped with 50 $\times$  objective at the State Key  
137 Laboratory of Continental Dynamics, Northwest University, Xi'an, China. Raman spectra were  
138 collected with an invia laser Raman spectrometer (Renishaw, UK) at 24 °C. The excitation  
139 wavelength is 514.5 nm (semiconductor laser), and the output power of the laser was set at 100 mW  
140 with a Renishaw edge filter. The 50X objective on a Leica DM LM microscope was used, and a  
141 grating with 1800 grooves/mm was selected. The spectral resolution (apparatus function) was  $\sim 3.0$   
142  $\text{cm}^{-1}$  determined by an emission spectrum from a neon lamp at  $\sim 918.6 \text{ cm}^{-1}$ .

## 143 **RESULTS**

### 144 **Optical, morphological, and physical properties of wenlanzhangite-(Y)**

145 Wenlanzhangite-(Y) is translucent to transparent. Reflectance data are given in Table 1 and Figure 4.  
146 The refractive index  $n$  of wenlanzhangite-(Y) is 2.17, which is calculated by  $N=Kd+1$  (K values  
147 from Mandarino 1981). The dispersion is medium with  $r < v$ , and the pleochroism is with X = brown,  
148 Y = dark brown, Z = brown black. The a: b: c ratio from single-crystal X-ray diffraction data is  
149 0.601: 0.968: 1. The colour, streak, lustre, and hardness (Mohs) are dark brown, yellow grey, vitreous,  
150 and ~4, respectively. The cleavage is good and parallel to {110}. The calculated density is 4.54 g/cm<sup>3</sup>  
151 based on the empirical formula and unit cell volume determined from single crystal XRD data.

## 152 **Chemical composition**

153 Wenlanzhangite-(Y) displays narrow ranges of SiO<sub>2</sub>, Al<sub>2</sub>O<sub>3</sub>, Y<sub>2</sub>O<sub>3</sub>, Dy<sub>2</sub>O<sub>3</sub>, Er<sub>2</sub>O<sub>3</sub>, Gd<sub>2</sub>O<sub>3</sub>, Yb<sub>2</sub>O<sub>3</sub>,  
154 Nd<sub>2</sub>O<sub>3</sub>, and Sm<sub>2</sub>O<sub>3</sub> contents, ranging from 16.07 to 16.63 wt%, 3.38 to 4.18 wt%, 18.55 to 19.59  
155 wt%, 3.93 to 4.46 wt%, 2.42 to 3.11 wt%, 1.88 to 2.34 wt%, 2.18 to 2.74 wt%, 1.86 to 2.27 wt%, and  
156 1.16–1.48 wt%, respectively. Sc<sub>2</sub>O<sub>3</sub>, Ho<sub>2</sub>O<sub>3</sub>, Ce<sub>2</sub>O<sub>3</sub>, Tb<sub>2</sub>O<sub>3</sub>, Tm<sub>2</sub>O<sub>3</sub>, and Pr<sub>2</sub>O<sub>3</sub> contents are low with  
157 0.15–0.66 wt%, 0.54–1.11 wt%, 0.26–0.50 wt%, 0.45–0.67 wt%, 0.38–0.80 wt%, and 0.08–0.28  
158 wt%, respectively (Table 2). The average empirical formula, calculated on the basis of 8 cations per  
159 formula unit (apfu), is  
160  $(Y_{1.26}Dy_{0.17}Er_{0.11}Gd_{0.09}Yb_{0.09}Nd_{0.09}Sm_{0.06}Sc_{0.04}Ho_{0.03}Ce_{0.02}Tb_{0.02}Tm_{0.02}Pr_{0.01})_{\Sigma 2.00}(V^{3+}_{1.46}Al_{0.54})_{\Sigma 2.00}V^{4+}$   
161  $_2(SiO_4)_2O_4(OH)_4$ . The type and amount of OH were determined from bond-valence calculations of O  
162 atoms in the crystal structure, and the Raman spectrum of wenlanzhangite-(Y) (Fig. 5). As for total  
163 REE and HREE contents, wenlanzhangite-(Y) has  $\Sigma$ REE concentrations of 2.50–2.98×10<sup>5</sup> ppm,  
164 with Y/Ho ratios (16–19, mean= 18), and Eu/Eu\* (0.21–0.32, mean= 0.26) ratios (Fig. 6; Table S1).

## 165 **Crystal structure**

166 Unit-cell parameters obtained from the single-crystal and selected-area electron using TEM  
167 diffraction (Fig. 7) data are:  $a = 5.9632(7)$  Å,  $b = 9.599(1)$  Å,  $c = 9.9170(9)$  Å,  $\alpha = 90.033(8)^\circ$ ,  $\beta =$   
168  $98.595(2)^\circ$ ,  $\gamma = 90.003(9)^\circ$ , and  $V = 561.28(10)$  Å<sup>3</sup>, and  $a = 5.948(1)$  Å,  $b = 9.616(1)$  Å,  $c = 9.916(1)$   
169 Å,  $\alpha = 90.00(1)^\circ$ ,  $\beta = 98.35(1)^\circ$ ,  $\gamma = 90.00(1)^\circ$ , and  $V = 561.14(3)$  Å<sup>3</sup>, respectively. The X-ray



170 powder diffraction data are shown in Table S2. The initial crystal structure determination was  
171 performed using OLEX2–1.3 (Dolomanov et al. 2009), and the refined structure model was solved  
172 with the SHELXT2014/5 directly and subsequently by SHELXL2016/6 with least square refinement  
173 (Sheldrick 2015a, b). Although the single-crystal XRD data indicate two possible crystal structures,  
174  $P-1$  and  $I2/a$ , the TEM results indicated that the SAED can only be indexed by a  $P-1$  structure and  
175 not  $I2/a$ . The structure was therefore solved in space group  $P-1$  (#2). Crystallographic data and  
176 refinement statistics are given in Table 3. The occupancies of atoms are refined toward minimum  $R_1$   
177 and show good agreement with the measured chemical composition. For simplicity, only Y and Dy  
178 are considered in the refinement for rare earth elements (REE), since they are the first two major  
179 elements according to microprobe analyses. The final atomic coordinates and displacement  
180 parameters are listed in Table 4, and selected bond lengths in Table 5. The bond–valence sums of  
181 atoms are presented in Table S3.

182 The structure of wenlanzhangite–(Y) is composed of  $a$ -axis-oriented chains of edge-sharing  
183  $[VO_6]$  octahedra linked by insular  $[SiO_4]$  tetrahedra, leaving open channels occupied by rare earth  
184 elements (Fig. 8). The octahedra could be divided into two types according to geometry. Type one  
185 ( $[V1O_6]$  and  $[V2O_6]$ ) are strongly distorted octahedra (DO) with respect to the major difference  
186 between the shortest V–O distance ( $\approx 1.7$  Å) and the longest V–O distance ( $\approx 2.4$  Å). Type two  
187 ( $[V3O_6]$ ,  $[V4O_6]$  and  $[V5O_6]$ ) are closer to regular octahedra (RO). Two different octahedra are  
188 distributed in different chains, respectively. Like the structure of jingwenite-(Y) (Liu et al. 2023), the  
189 two types are dominated by  $V^{4+}$  in  $[V1O_6]$  and  $[V2O_6]$ , and by  $V^{3+}$  in  $[V3O_6]$ ,  $[V4O_6]$  and  $[V5O_6]$   
190 for wenlanzhangite-(Y). The  $[SiO_4]$  tetrahedra share corners with two separate chains of RO and  
191 share corners with two neighboring octahedra in the same chains of DO. Rare earth elements are 8–  
192 coordinated and occupy open channels along the  $b$ -axis. Bond valence calculations show that  
193 hydrogen atoms are attached with four oxygen atoms (O13, O14, O15, O16), leading to the ideal  
194 crystal chemical formula  $Y_2V^{3+}_2V^{4+}_2(SiO_4)_2O_4(OH)_4$ . The atomic occupancies for each site are

195 described below:

196 **(1) V1 and V2 sites:** These two sites are 6-coordinated. The bond valence calculations of  
197 jingwenite-(Y) (Liu et al. 2023) have indicated that a similar site is dominated by  $V^{4+}$ . This situation  
198 is consistent in wenlanzhangite-(Y). But, during the structure refinement of wenlanzhangite-(Y),  
199 slightly weaker scatterers of X-rays than V are noticed at both sites, indicating that some  
200 heterovalent  $Al^{3+}$  can co-occupy the V1 and V2 sites. This is also confirmed by broadband  
201 viscoelastic spectroscopy. The edge-sharing chains of  $[V^{4+}O_6]$  octahedra also occur in synthetic  $VO_2$   
202 (C2/m) (Marezio et al. 1972) and  $VO_2$  (P2<sub>1</sub>/c) (Longo and Kierkegaard 1970), in which V–O bond  
203 lengths vary from 1.73 Å to 2.13 Å.

204 **(2) V3, V4 and V5 sites:** These three sites are 6-coordinated.  $V^{3+}$  and  $Al^{3+}$  are mixed in **V5**  
205 sites and structure refinement result shows they are all dominated by  $V^{3+}$ .

206 **(3) Si sites:** there are two distinct Si positions, all tetrahedrally coordinated by oxygen anions.  
207 The average Si–O distances are 1.654 and 1.650 Å, which is longer than the normally observed range  
208 in silicates.

209 **(4) REE sites:** Y1 and Y2 sites are 8-coordinated and dominated by  $Y^{3+}$ . Dy3 and Dy4 sites are  
210 dominated by □, because they only possess 7.34 and 7.28  $e^-$ . They are recognized as trace amounts  
211 of  $Dy^{3+}$  rather than  $Y^{3+}$  due to the average bond length of Dy3–O being longer than either Y1–O or  
212 Y2–O. The small amounts of additional rare earths balance the valence state that is insufficient due  
213 to the substitution of  $Al^{3+}$  for tetravalent elements (e.g.,  $V^{4+}$ ).

214 Therefore, the crystal structure of wenlanzhangite-(Y) is sufficiently close to that of  
215 jingwenite-(Y) (Liu et al. 2023) that it should be classified within the same group of jingwenite-(Y)  
216 with a Dana classification number 52.4.10.2.

## 217 **Raman spectrum**

218 The Raman spectrum of wenlanzhangite-(Y) shows the bands of O–H stretching vibrations at 3572  
219  $cm^{-1}$ , the bands of Si–O stretching vibrations at 829, 893, and 951  $cm^{-1}$ , and the bands of Al–O, V–O,

220 and Y–O vibrations in the range of 100–600 cm<sup>-1</sup> (Liu et al. 2023).

## 221 DISCUSSION

222 In contrast to jingwenite–(Y) with 21.65 wt% VO<sub>2</sub>, 4.04 wt% V<sub>2</sub>O<sub>3</sub>, and 10.85 wt% Al<sub>2</sub>O<sub>3</sub>,  
223 wenlanzhangite–(Y) displays similar VO<sub>2</sub> (22.05–22.60 wt%) but higher V<sub>2</sub>O<sub>3</sub> (14.07–15.42 wt%)  
224 and lower Al<sub>2</sub>O<sub>3</sub> (3.38–4.18 wt%) contents. Moreover, the crystal system, space group, and unit cell  
225 of wenlanzhangite–(Y) are all distinct from those of jingwenite–(Y) (Table 6) (Fig. 8). The structure  
226 of jingwenite–(Y) is composed of *b*-axis-oriented chains of octahedra consisting of edge-sharing Al  
227 (V, Fe)–O octahedra and V (Ti)–O octahedra linked by insular Si–O tetrahedra (Liu et al. 2023). In  
228 the chains of Al–O octahedra, two alternative cation sites, Al1 and Al2, share edges O4–O4 and O7–  
229 O7. Both sites are dominated by Al but with the incorporation of Fe<sup>3+</sup> and V<sup>3+</sup>, more in Al2 than in  
230 Al1. On this basis, V mainly occurs as V<sup>4+</sup> in jingwenite–(Y), while V<sup>3+</sup> can substitute for Al<sup>3+</sup> and  
231 Fe<sup>3+</sup>. Both V<sup>3+</sup> and V<sup>4+</sup> are dominant cations in wenlanzhangite–(Y) with less Al<sup>3+</sup> and Fe<sup>3+</sup>. The  
232 differences in space group and unit cell are the results of the splitting of V sites. Given the measured  
233 variation in calculated V<sup>3+</sup>/(V<sup>3+</sup>+Al), there is likely a solid–solution series extending from  
234 endmember, Y<sub>2</sub>Al<sub>2</sub>V<sup>4+</sup><sub>2</sub>(SiO<sub>4</sub>)<sub>2</sub>O<sub>4</sub>(OH)<sub>4</sub>, toward another endmember, Y<sub>2</sub>V<sup>3+</sup><sub>2</sub>V<sup>4+</sup><sub>2</sub>(SiO<sub>4</sub>)<sub>2</sub>O<sub>4</sub>(OH)<sub>4</sub>.  
235 Compositions across this solid solution are present in the zoned crystal shown in Fig. 3b, in which  
236 V<sup>3+</sup>/(V<sup>3+</sup>+Al+Fe<sup>3+</sup>), ranges from 0.19 in jingwenite–(Y) up to 0.76 (equivalent to 1.53 a.p.f.u. V<sup>3+</sup>) in  
237 wenlanzhangite–(Y) (Fig. 6b) (Tables 4 and S1). The observed intracrystal zoning is likely an  
238 expression of an evolutionary process involving changes in the composition of hydrothermal fluid  
239 and/or fluid parameters over time. Moreover, the structure of a V–enriched analogue of jingwenite–  
240 (Y), Y<sub>2</sub>AlV<sup>3+</sup><sub>3</sub>V<sup>4+</sup><sub>2</sub>(SiO<sub>4</sub>)<sub>2</sub>O<sub>4</sub>(OH)<sub>4</sub>, has been determined in which the two nearly regular octahedra  
241 sites are dominated by Al<sup>3+</sup> and V<sup>3+</sup>, respectively.

## 242 IMPLICATIONS

243 In general, V can be dissolved and transported in oxidized fluids as V<sup>5+</sup>. In turn, V<sup>4+</sup> and V<sup>3+</sup> are

244 insoluble in hydrothermal fluids and preferentially partition into mineral phases (Fischer 1973;  
245 Huang et al. 2015b). Thus, like HREE and U, V is also likely leached and transported as  $V^{5+}$  by  
246 oxidized fluids, and then reduced to insoluble  $V^{4+}$  or  $V^{3+}$  upon contact with organic- and apatite-rich  
247 beds in the overlying dolostone/limestone, precipitating and partitioned into jingwenite-(Y). The  
248 presence of wenlanzhangite-(Y) as rims on normal jingwenite-(Y) indicates an evolution to a  
249 relatively more reduced hydrothermal environment causing conversion, in which  $V^{5+}$  is reduced to  
250  $V^{4+}$  and additional  $V^{3+}$ . This interpretation is also suggested by the higher Eu/Eu\* ratios in  
251 wenlanzhangite-(Y) (Fig. 6c), as well as by the negative correlation between measured  $Fe^{3+}$  and  
252 calculated  $V^{3+}$ . Dissolution of Fe-Mn-rich particles or oxyhydroxides can lead to fractionation of Y  
253 and Ho due to the higher marine particle-reactivity of Ho compared to Y (Bau et al. 1996). Fe-Mn  
254 oxyhydroxides facilitate dissolution under anoxic conditions, yielding low Y/Ho ratios (<28) in  
255 hydrothermal systems (Planavsky et al. 2010). Therefore, the lower Y/Ho ratios in wenlanzhangite-  
256 (Y) (Fig. 6c) can be interpreted as a response to greater volumes of Fe-Mn-rich oxyhydroxides in  
257 dolostone/limestone and red sandstone dissolved in relatively reduced ore-forming fluids during  
258 fluid-rock reaction. All these observations suggest that wenlanzhangite-(Y) and jingwenite-(Y) have  
259 great potential as proxies for tracing the redox state of ore-formation. Temperature and pressure  
260 conditions of wenlanzhangite-(Y) formation are estimated to be 110–287 °C and 50 MPa,  
261 respectively, based on fluid-inclusion studies (Liu 1997; Jiang et al. 2016).

## 262 ACKNOWLEDGMENTS

263 This research was jointly funded by the National Natural Science Foundation of China (grants  
264 42272070, 42130102, 42242201, and 42102080), the Young Star of Science and Technology Plan  
265 Projects in Shaanxi Province, China (Grant 2023KJXX-037) and the Natural Science Basic Research  
266 Program in Shaanxi Province of China (2022JC-DW5-01). The authors thank Dr. Yuan Cheng,  
267 Instrumentation and Service Center for Molecular Sciences, Westlake University, for the reflectance  
268 measurement. We are grateful to the editors Don Baker and Paolo Lotti, and two anonymous

269 reviewers for their constructive and critical comments and suggestions.

## 270 REFERENCES

- 271 Bao, Z.A., Yuan, H.L., Zong, C.L., Liu, Y., Chen, K.Y., and Zhang, Y.L. (2016) Simultaneous  
272 determination of trace elements and lead isotopes in fused silicate rock powders using a boron  
273 nitride vessel and fsLA–(MC)–ICP–MS. *Journal of Analytical Atomic Spectrometry*, 31, 1012.
- 274 Bau, M., Koschinsky, A., Dulski, P., and Hein, J.R. (1996) Comparison of the partitioning behaviours  
275 of yttrium, rare earth elements, and titanium between hydrogenetic marine ferromanganese  
276 crusts and seawater. *Geochimica et Cosmochimica Acta*, 60, 1709–1725.
- 277 Chen, M.H., Ke, C.H., Tian, Y.F., Chen, G., Ma, K.Z., Ma, S.X., Peng, Y.X., and Zhang, W. (2021)  
278 Sedimentary–exhalative massive sulfide deposits in shallow marine environment: a case study  
279 from Yushui copper deposit, Guangdong Province. *Acta Geologica Sinica*, 95, 1774–1791 (in  
280 Chinese with English abstract).
- 281 Dahlkamp, F.J. (2010) Uranium deposits of the world–USA and Latin America. Berlin, Germany,  
282 Springer, 423 p.
- 283 Dolomanov, O.V., Bourhis, L.J., Gildea, R.J., Howard, J., and Puschmann, H. (2009) Olex2: a  
284 complete structure solution, refinement and analysis program. *Journal of Applied*  
285 *Crystallography*, 42, 339–341.
- 286 Fischer, R.P. (1973) Vanadium. In Brobst, D.A., and Pratt, W.P., Eds., *United States Mineral*  
287 *Resources: U.S. Geological Survey Professional Paper*, 820, 679–688.
- 288 Huang, Y., Sun, X.M., Shi, G.Y., Sa, R.N., Guang, Y., Jiang, X.D., and Que, H.H. (2015a) Re–Os  
289 dating of sulfides from the Yushui Cu–polymetallic deposit in eastern Guangdong Province,  
290 South China. *Ore Geology Reviews*, 70, 281–289.
- 291 Huang, J.H., Huang, F., Evans, L., and Glasauer, S. (2015b) Vanadium: Global (bio) geochemistry.  
292 *Chemical Geology*, 417, 68–89.
- 293 Jiang, B.B., Zhu, X.Y., Cheng, X.Y., Wang, H. (2016) Characteristics and geological significance of

- 294 fluid inclusions in the Yushui copper polymetallic deposit, Guangdong Province. *Geology in*  
295 *China* 43, 2163–2172 (in Chinese with English abstract).
- 296 Liu, J.Q. (1997) Thermobarogeochemistry, ore-forming age and genesis study for the Yushui  
297 copper-rich multimetal deposit in Meixian county, Guangdong Province, Southern China.  
298 *Geology and Mineral Resources of South China*, 1, 37-50 (in Chinese with English abstract)
- 299 Liu, P., Gu, X.P., Zhang, W.L., Hu, H., Chen, X.D., Wang, X.L., Song W.L., Yu, M., and Cook, N.J.  
300 (2023) Jingwenite-(Y) from the Yushui Cu deposit, South China: the first occurrence of a V–  
301 HREE-bearing silicate mineral. *American Mineralogist*, 108–196.
- 302 Liu, Y.S., Hu, Z.C., Gao, S., Liu, Y.S., Hu, Z.C., Gao, S., Günther, D., Xu, J., Gao, C.G., and Chen,  
303 H.H. (2008) In situ analysis of major and trace elements anhydrous minerals by LA-ICP-MS  
304 without applying an internal standard. *Chemical Geology*, 257, 34–43.
- 305 Longo, J.M., and Kierkegaard, P. (1970) A refinement of the structure of VO<sub>2</sub>. *Acta Chemica*  
306 *Scandinavica*, 24, 420–426.
- 307 Mandarino, J.A. (1981) The Gladstone–Dale relationship: Part IV, The compatibility concept and its  
308 application. *The Canadian Mineralogist*, 19, 441–450.
- 309 Marezio, M., McWhan, D.B., Remeika, J.P., and Dernier, P.D. (1972) Structural aspects of the  
310 metal–insulator transition in Cr-doped VO<sub>2</sub>. *Physical Review B: Solid State*, 5, 2541–2551.
- 311 Momma, K., and Izumi, F. (2011) VESTA 3 for three-dimensional visualization of crystal,  
312 volumetric and morphology data. *Journal of Applied Crystallography*, 44, 1272–1276.
- 313 Northrop, H.R., Goldhaber, M.B., Landis, G.P., Unruh, J.W., Reynolds, R.L., Campbell, J.A., Wanty,  
314 R.B., Grauch, R.I., Whitney, G., and Rye, R.O. (1990) Genesis of the tabular-type vanadium–  
315 uranium deposits of the Henry basin, Utah. *Economic Geology*, 85, 215–269.
- 316 Planavsky, N., Bekker, A., Rouxel, O.J., Kamber, B., Hofmann, A., Knudsen, A., and Lyons, T.W.  
317 (2010) Rare earth element and yttrium compositions of Archean and Paleoproterozoic Fe  
318 formations revisited: new perspectives on the significance and mechanisms of deposition.

- 319            *Geochimica et Cosmochimica Acta*, 74, 6387–6405.
- 320    Shawe, D.R. (2011) Uranium–vanadium deposits of the Slick Rock district, Colorado. U.S.  
321            Geological Survey Professional Paper, 576–F, 67.
- 322    Sheldrick, G.M. (2015a) SHELXT–Integrated space–group and crystal structure determination. *Acta*  
323            *Crystallographica*, A71, 3–8.
- 324    Sheldrick, G.M. (2015b) Crystal structure refinement with SHELX. *Acta Crystallographica*, C71, 3–  
325            8.
- 326    Weeks, A.D., Coleman, R.G., and Thompson, M.E. (1959) Summary of the ore mineralogy, part 5 of  
327            Garrels, R.M., and Larsen, E.S. III, comps., *Geochemistry and mineralogy of the Colorado*  
328            *Plateau uranium ores* (3<sup>rd</sup> ed.). U.S. Geological Survey Professional Paper, 320, 65–79.

## FIGURE CAPTIONS

329

330 **Fig 1.** (a) Geological map of the Yushui deposit (after Huang et al., 2015a). (b) Geological cross  
331 section of the exploration line a–b (from Chen et al., 2021).

332 **Fig 2.** (a) Stratigraphic column of the Yushui deposit. (b) Photograph of drillcore of red sandstone;  
333 (c)–(e) Photographs of bedded orebody. (f) Photomicrograph of disseminated ore in red sandstone. (g)  
334 Photograph of vein–style orebody in red sandstone. Bn–bornite; Cc–chalcocite; Ccp–chalcopyrite.

335 **Fig 3.** Photomicrographs showing the occurrence and mineral association of wenlanzhangite–(Y) and  
336 jingwenite–(Y) (Jw–Y). (a). Wenlanzhangite–(Y) (Wlz–Y) as a dark brown, 100  $\mu\text{m}$ –thick core on  
337 jingwenite–(Y) with bornite (Bn), roscoelite (Rcl), and thortveitite (Tv). (b) Back–scattered electron  
338 image of euhedral jingwenite–(Y) and wenlanzhangite–(Y) crystals with bornite, in reflected light,  
339 parallel nicols. (c) and (d). EPMA element (Al and V) maps of the marked box shown in (b). Note  
340 grain–scale compositional zoning in (b) reflecting variation from typical jingwenite–(Y),  
341  $\text{Y}_2\text{Al}_2\text{V}^{4+}_2(\text{SiO}_4)_2\text{O}_4(\text{OH})_4$ , to wenlanzhangite–(Y).

342 **Fig 4.** Reflectance data for wenlanzhangite–(Y) in air. The reflectance values (R%) are plotted versus  
343 wavelength in nm.

344 **Fig 5.** Raman spectra for wenlanzhangite–(Y).

345 **Fig 6.** (a). Chondrite–normalized rare earth element (REE) fractionation patterns for jingwenite–(Y)  
346 and wenlanzhangite–(Y). (b).  $\text{Y}/(\text{REE}+\text{Y}+\text{Sc})$  vs.  $\text{V}^{3+}/(\text{V}^{3+}+\text{Al}+\text{Fe}^{3+})$  ratio plot. (c).  $\text{Eu}/\text{Eu}^*$  vs.  $\text{Y}/\text{Ho}$   
347 ratio plots for jingwenite–(Y) and wanlanzhangite–(Y).

348 **Fig 7.** SAED patterns of wenlanzhangite–(Y) from 4 different zone axes.

349 **Fig 8.** Crystal structure of wenlanzhangite–(Y) (a) and jingwenite–(Y) (b), plotted with VESTA  
350 (Momma and Izumi, 2011).

351



## TABLE CAPTIONS

352

353 **Table 1.** Reflectance data for wenlanzhangite-(Y).

354 **Table 2.** Major-element data for wenlanzhangite-(Y) compared with jingwenite-(Y) (wt.%).

355 **Table 3.** Information on crystal and structural refinement for wenlanzhangite-(Y).

356 **Table 4.** Site, Wyckoff position (*W.p.*), site occupancy (s.o.), fractional atomic coordinates, and  
357 equivalent isotropic (and anisotropic) displacement parameters ( $\text{\AA}^2$ ) for wenlanzhangite-(Y).

358 **Table 5.** Selected bond lengths ( $\text{\AA}$ ) for wenlanzhangite-(Y).

359 **Table 6.** Comparison between wenlanzhangite-(Y) and jingwenite-(Y).

360

## SUPPLEMENTARY TABLE CAPTIONS

361 **Table S1** REE contents in jingwenite-(Y) and wenlanzhangite-(Y) as determined by LA-ICP-MS.

362 **Table S2.** X-ray powder diffraction data ( $d$  in  $\text{\AA}$ ,  $I$  in %) for wenlanzhangite-(Y).

363 **Table S3.** Calculated bond valences (*v.u.*) for atoms in wenlanzhangite-(Y).

364

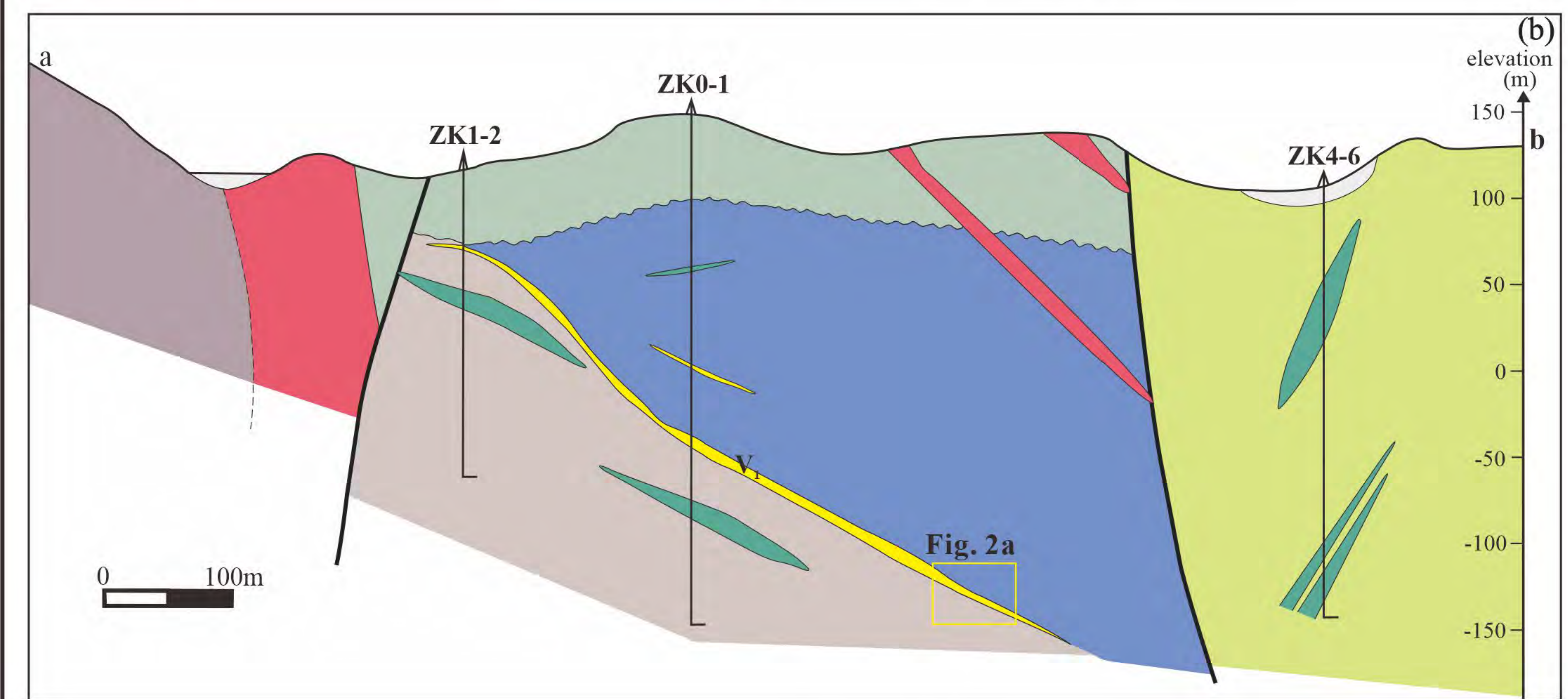
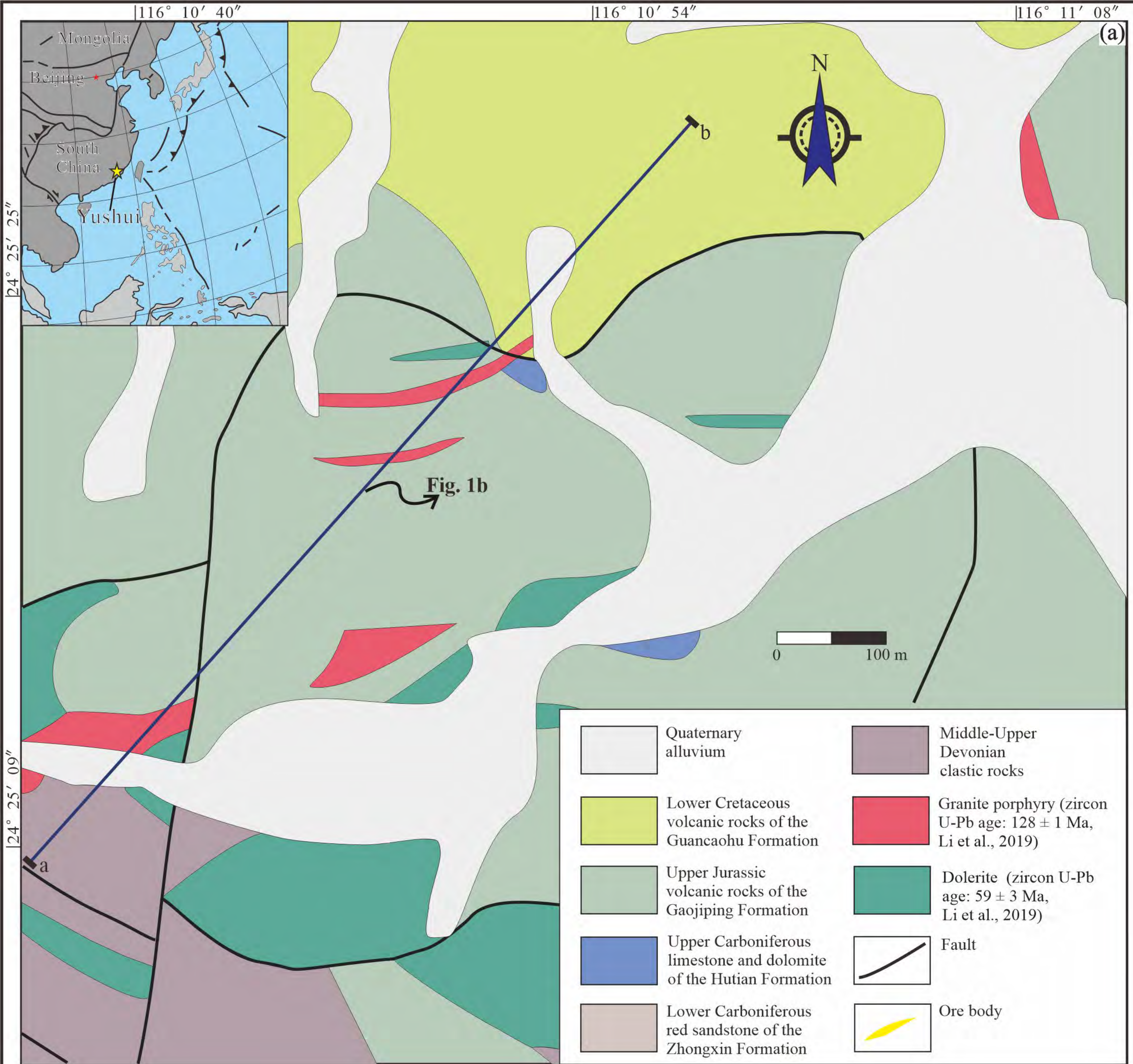


Fig. 1 revision 2

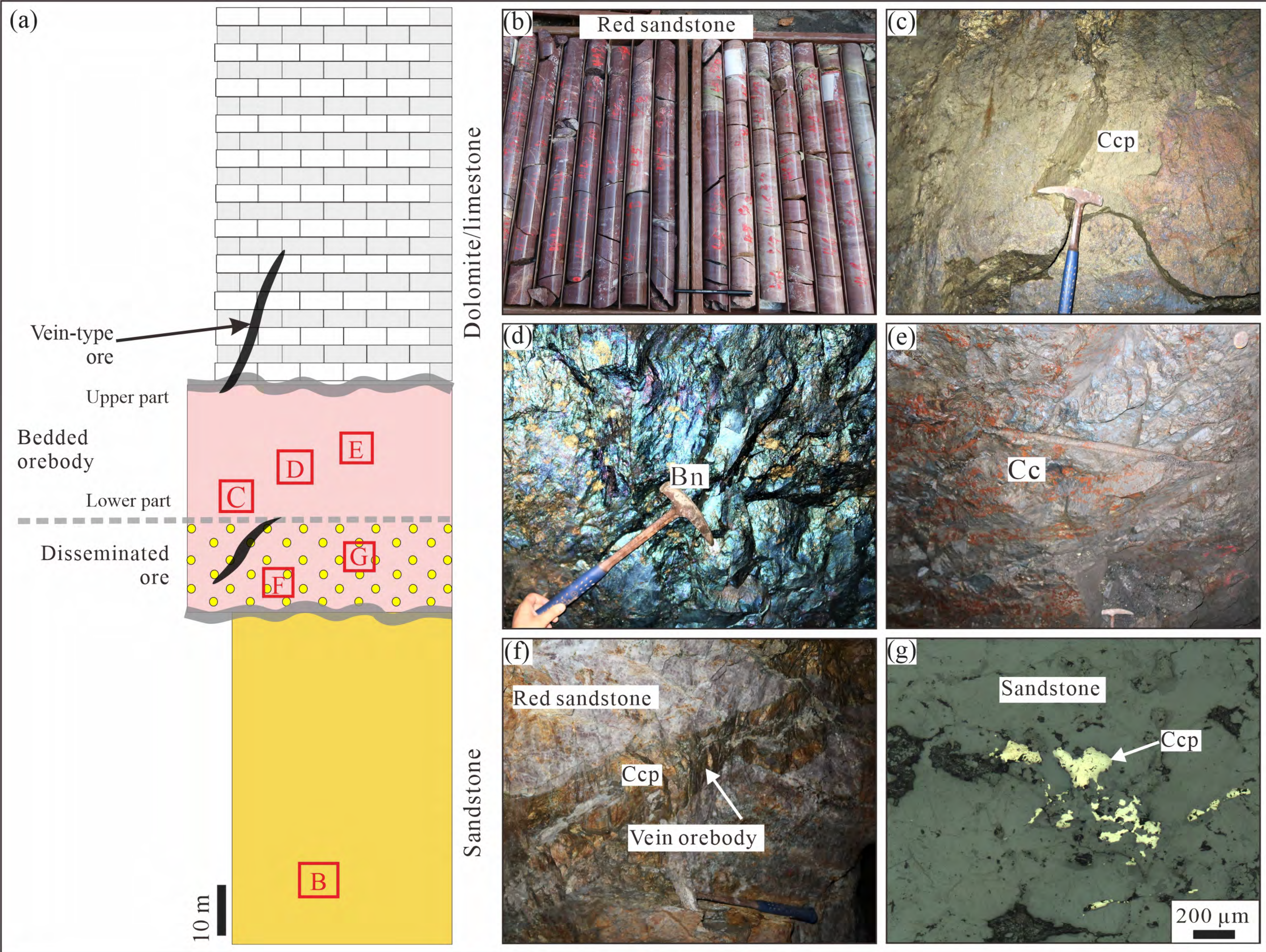


Fig. 2 revision 2

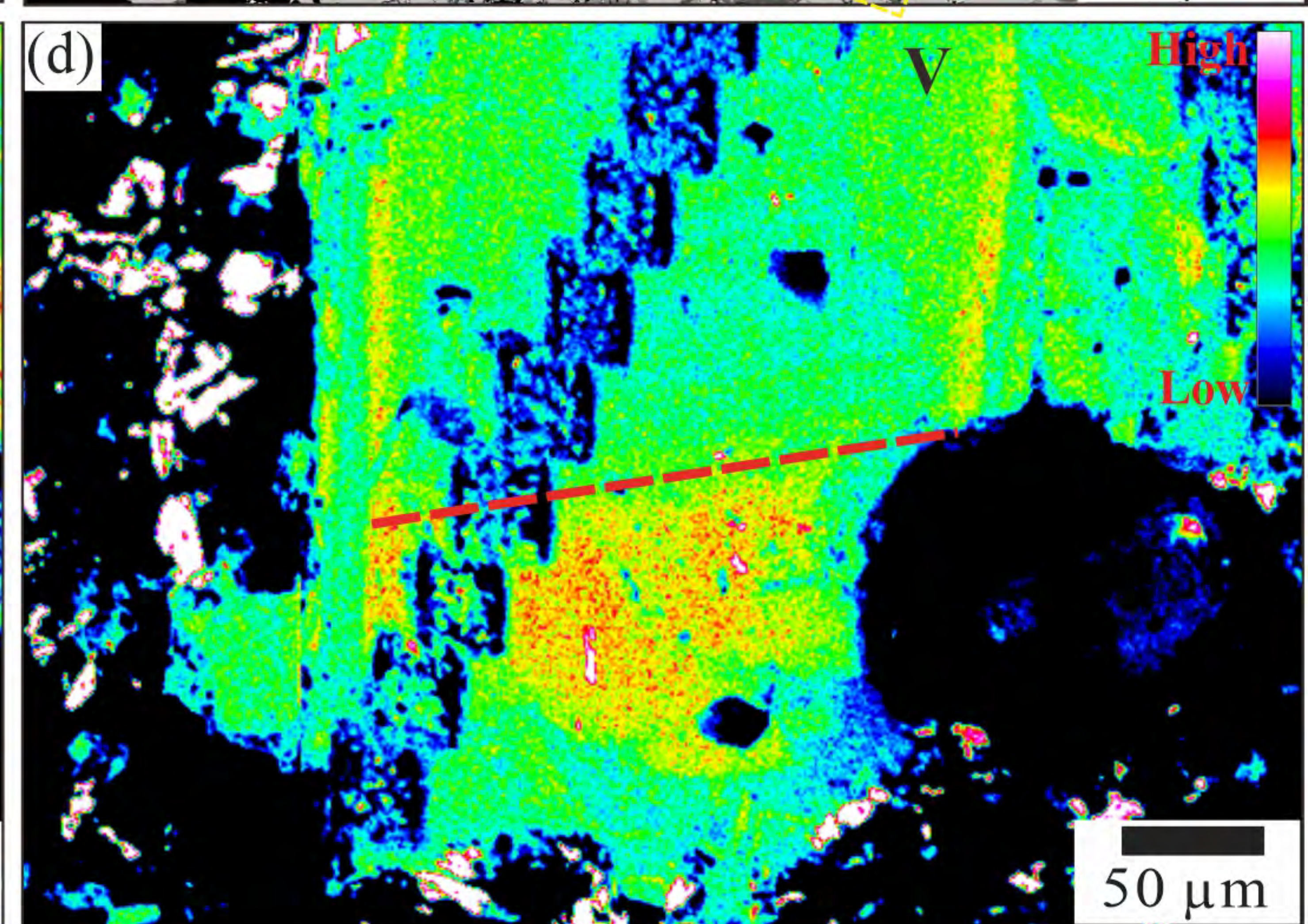
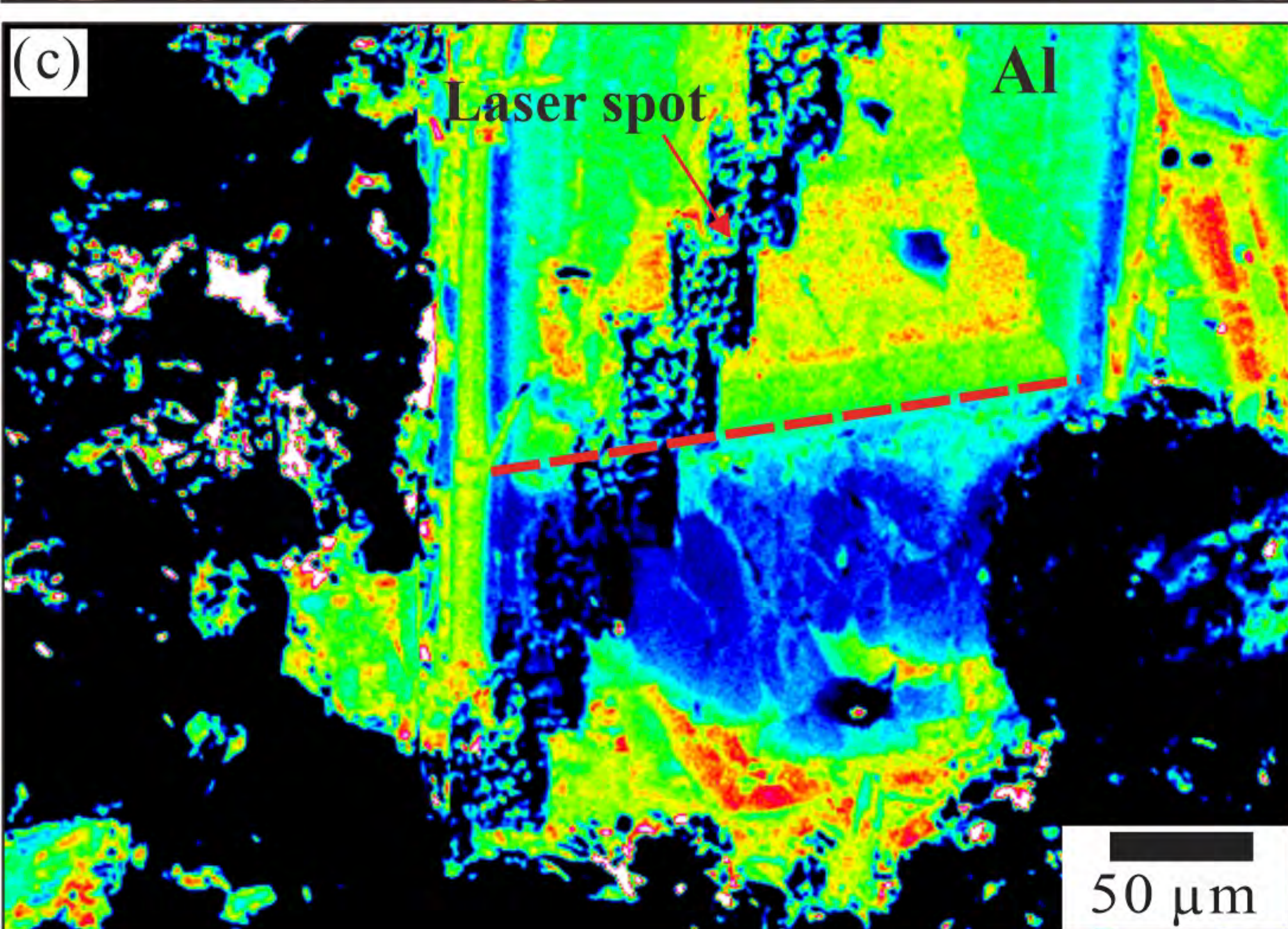
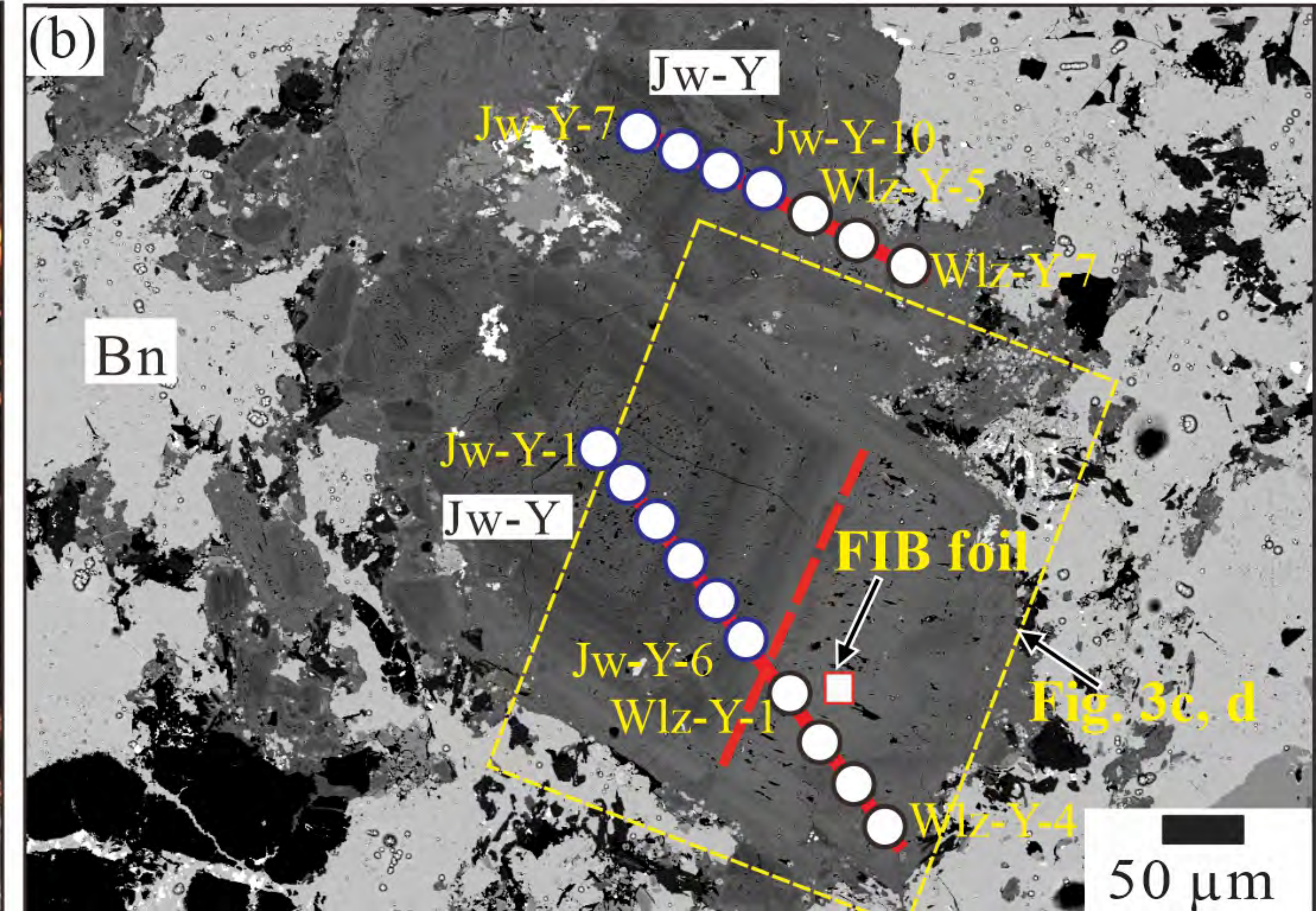
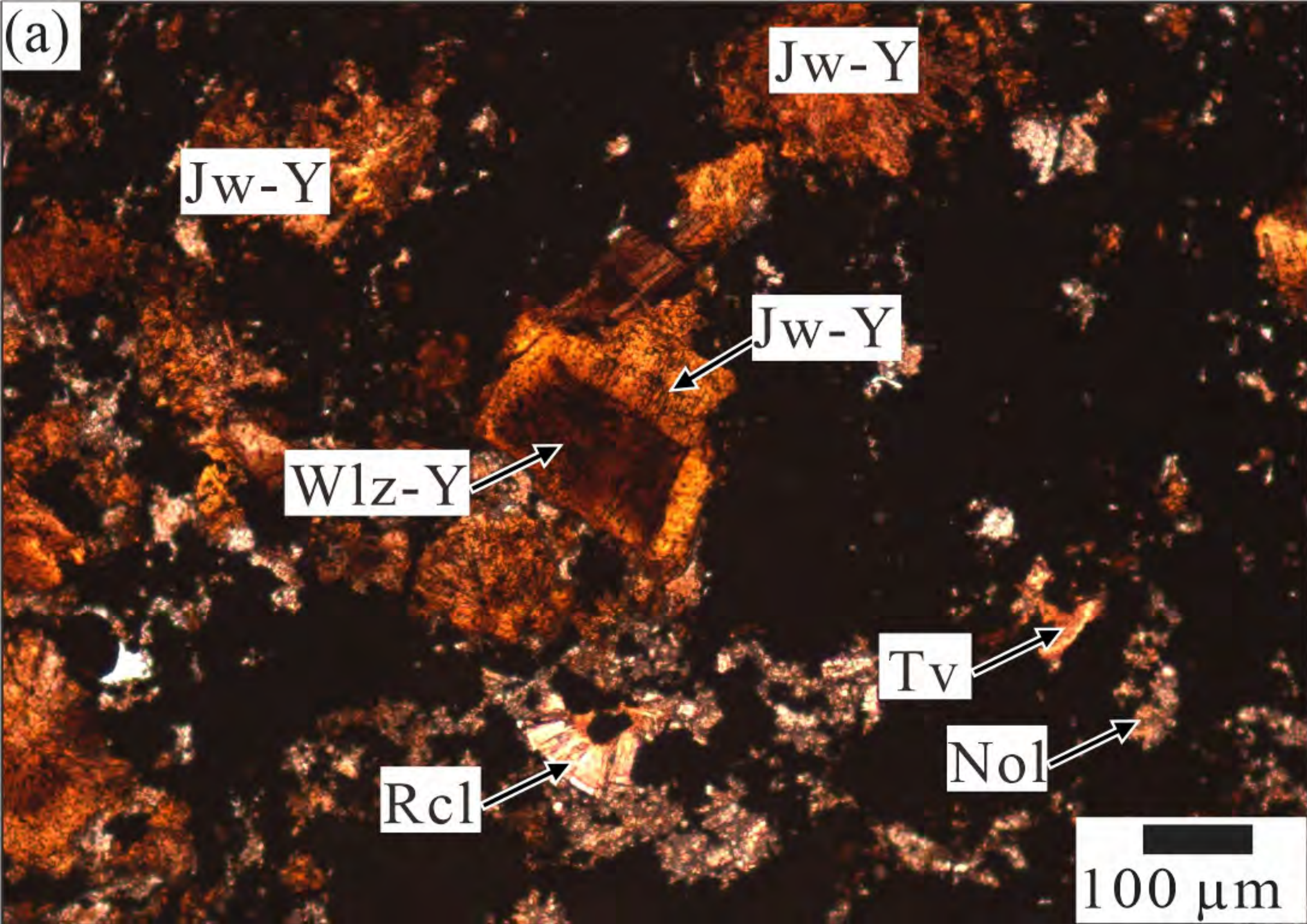


Fig. 3 revision 2

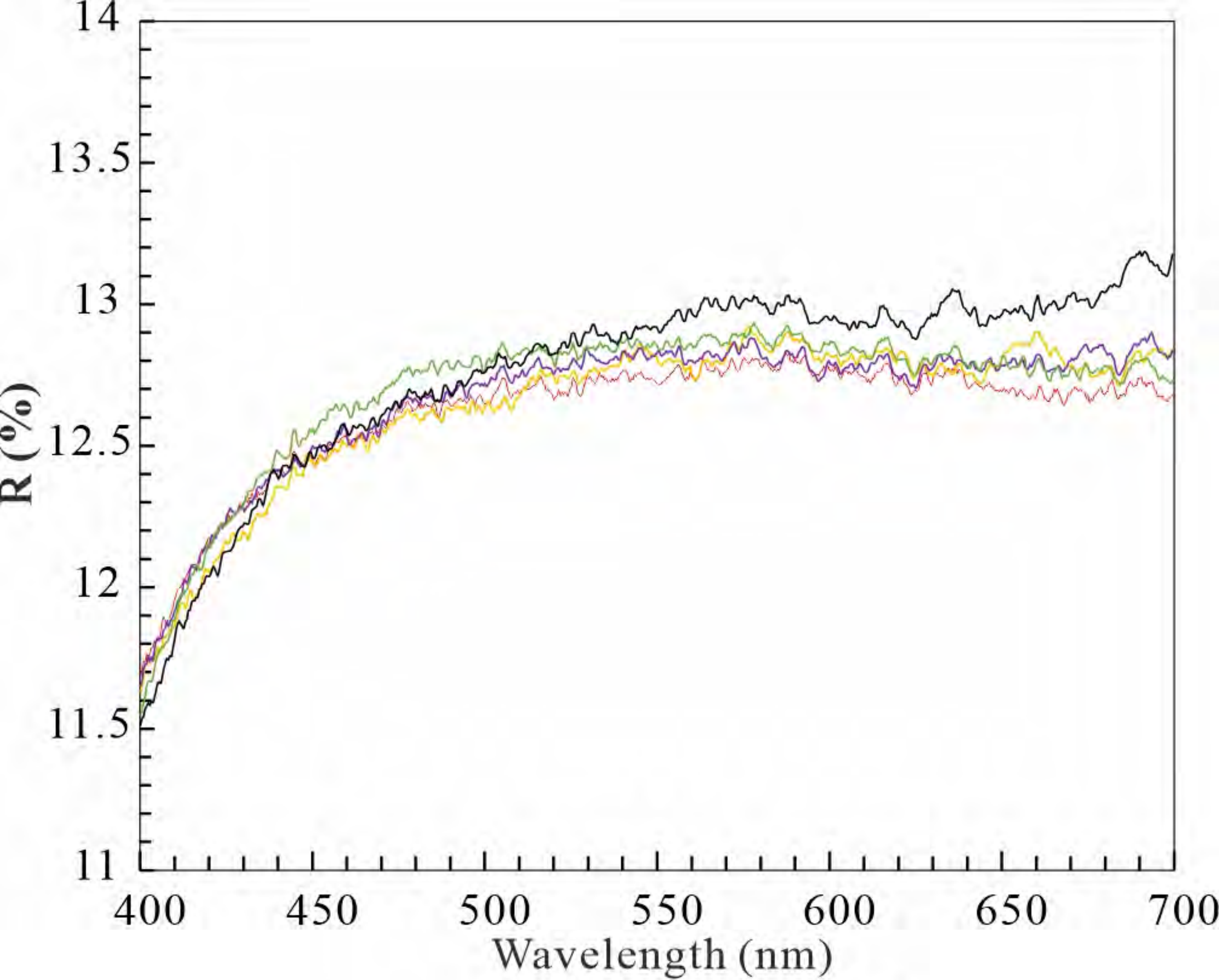


Fig. 4 revision 2

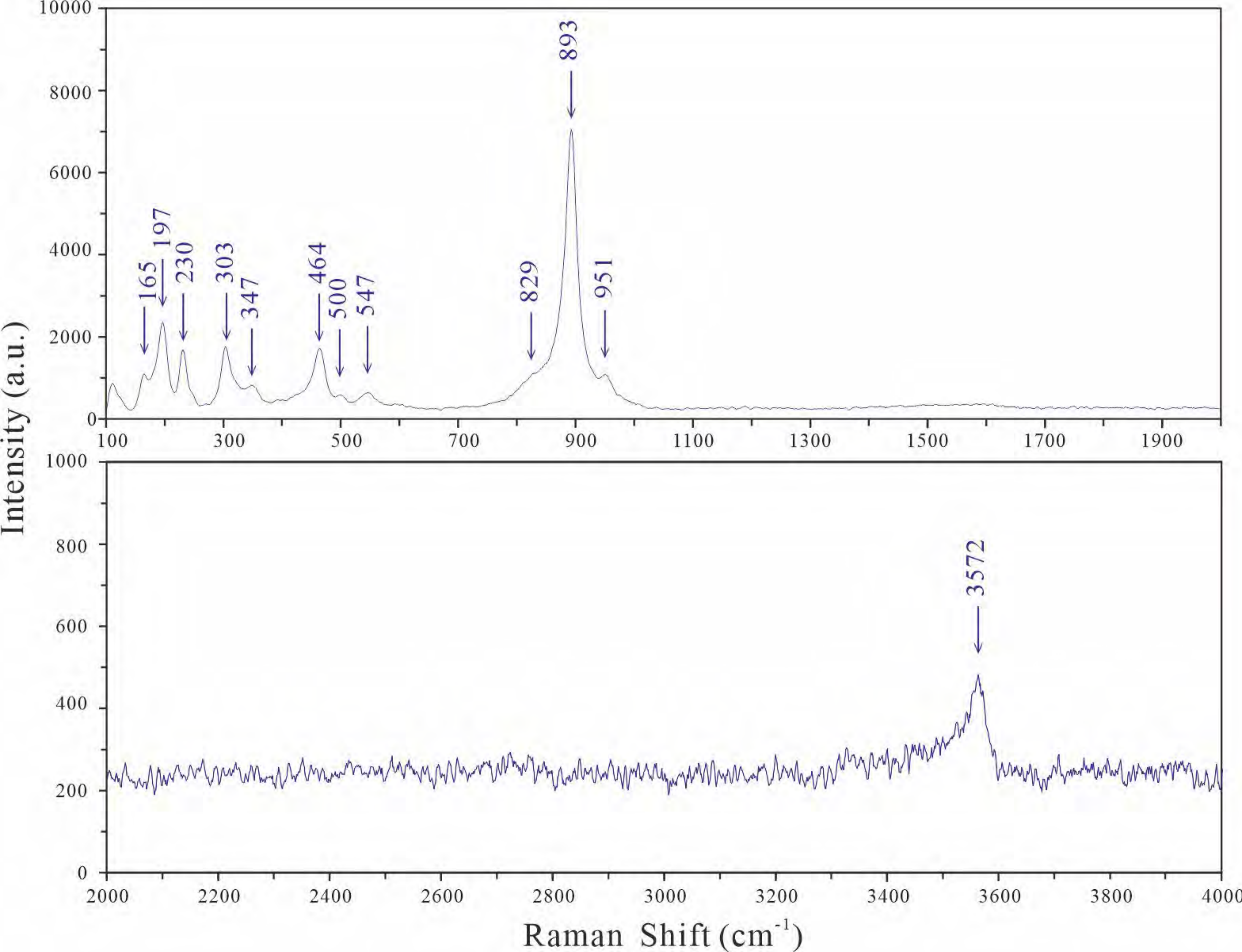


Fig. 5 revision 2

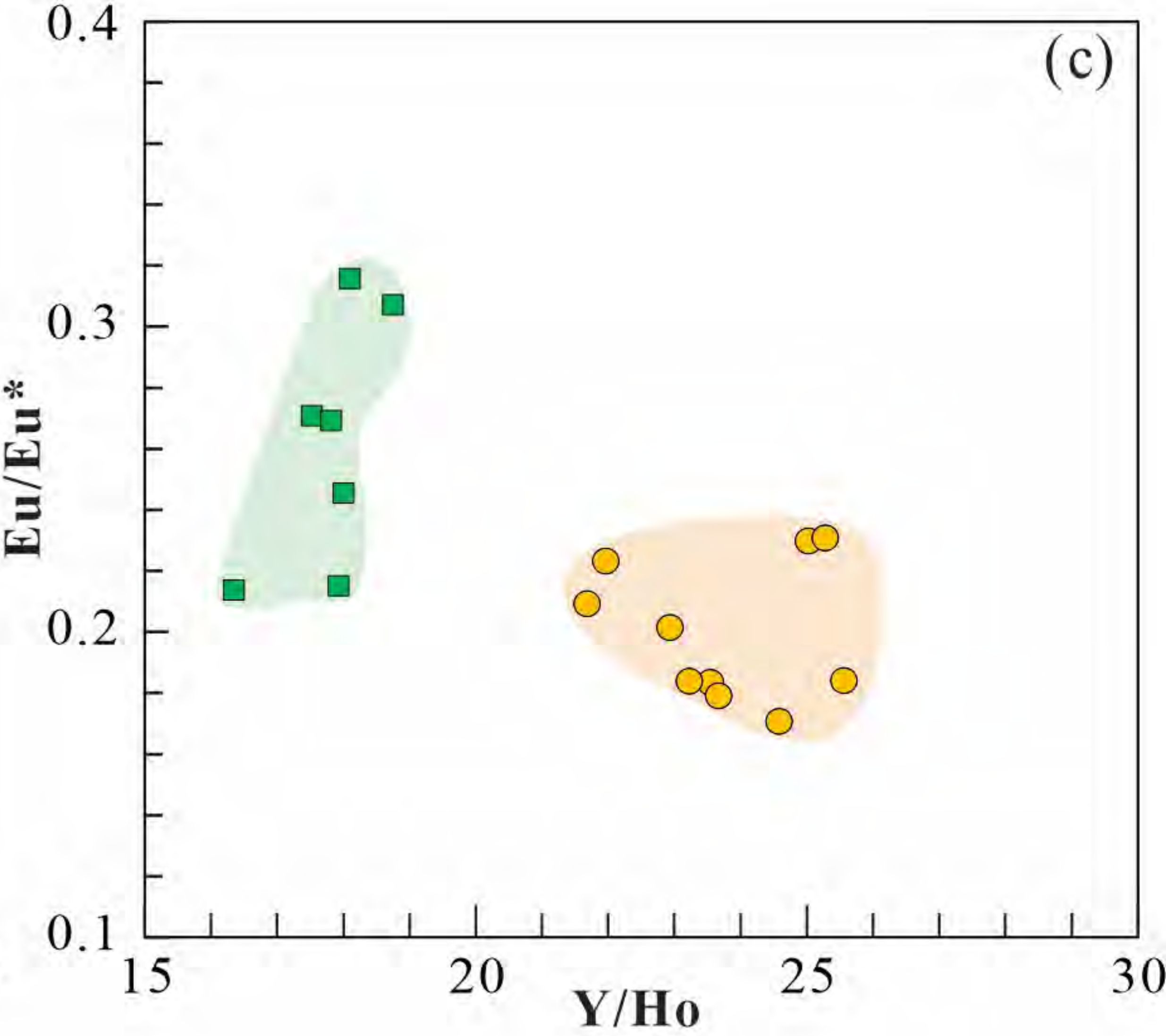
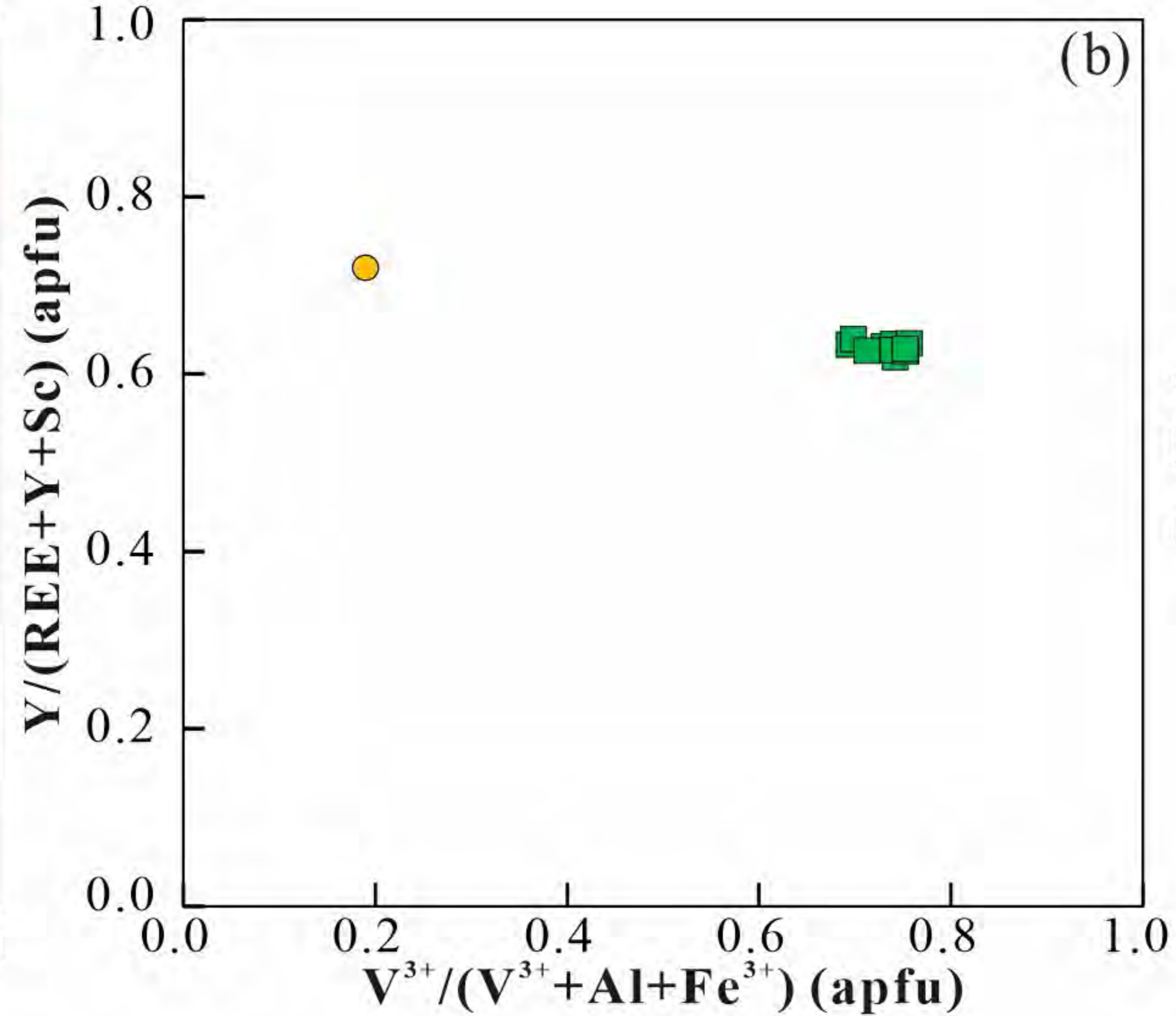
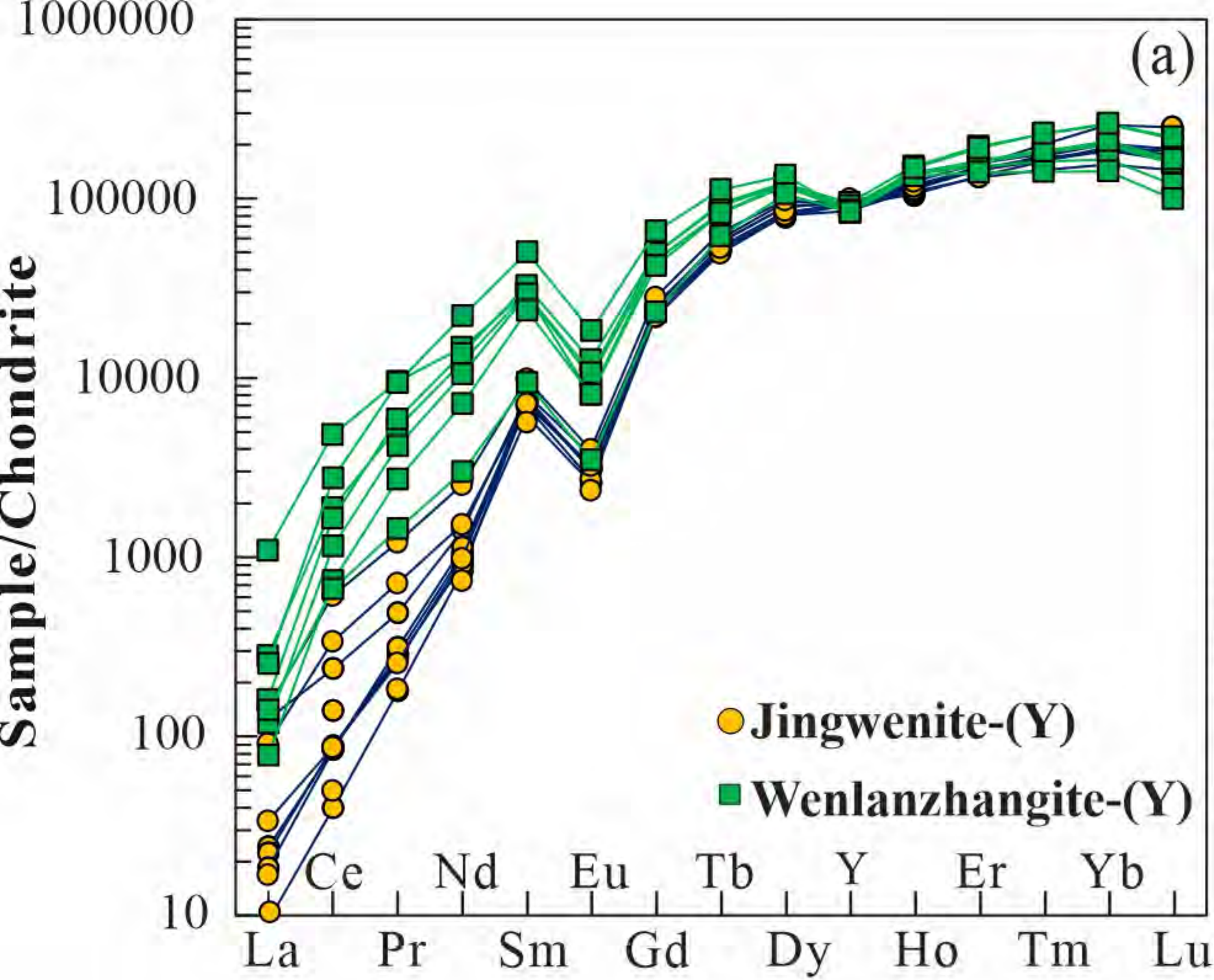


Fig. 6 revision 2

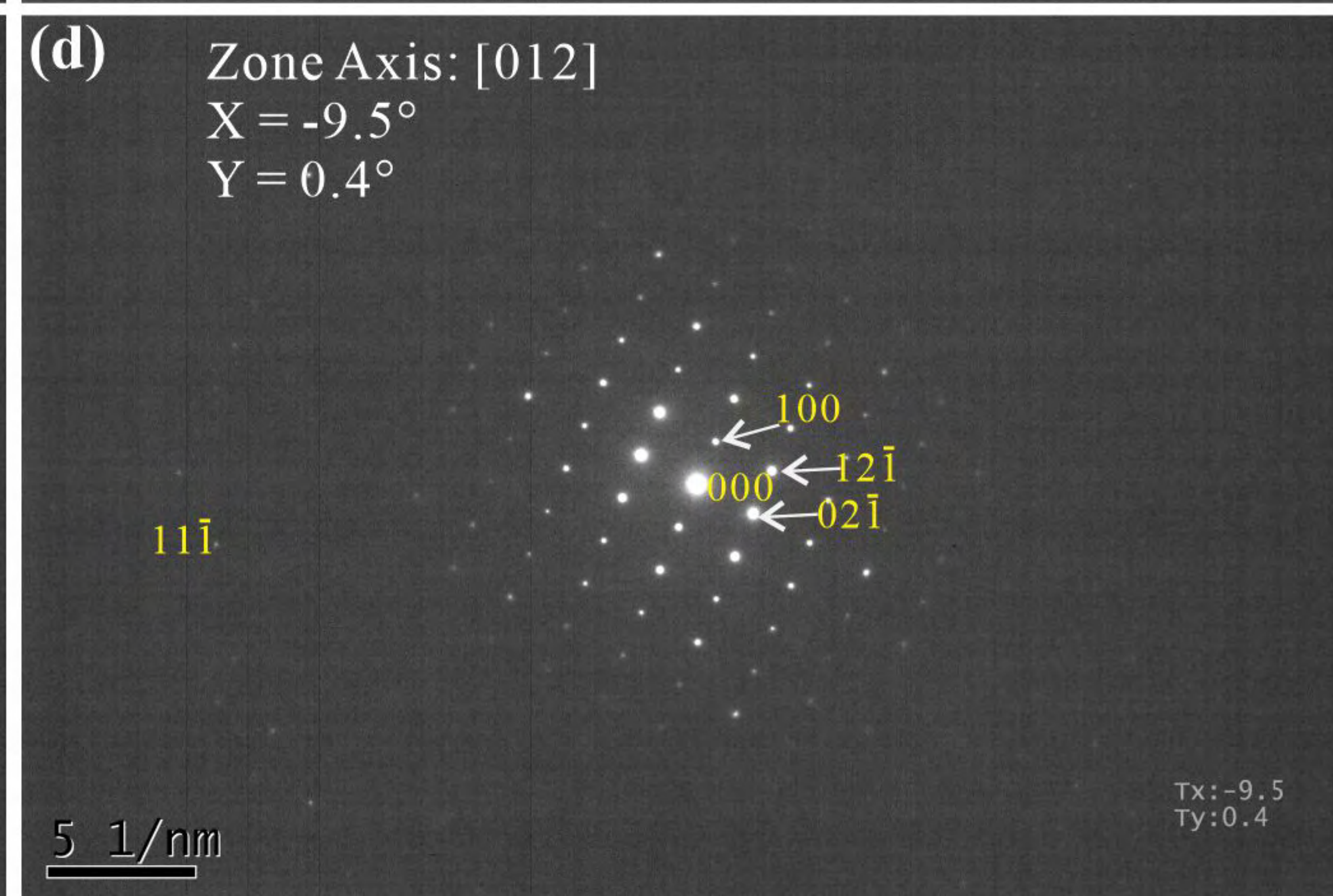
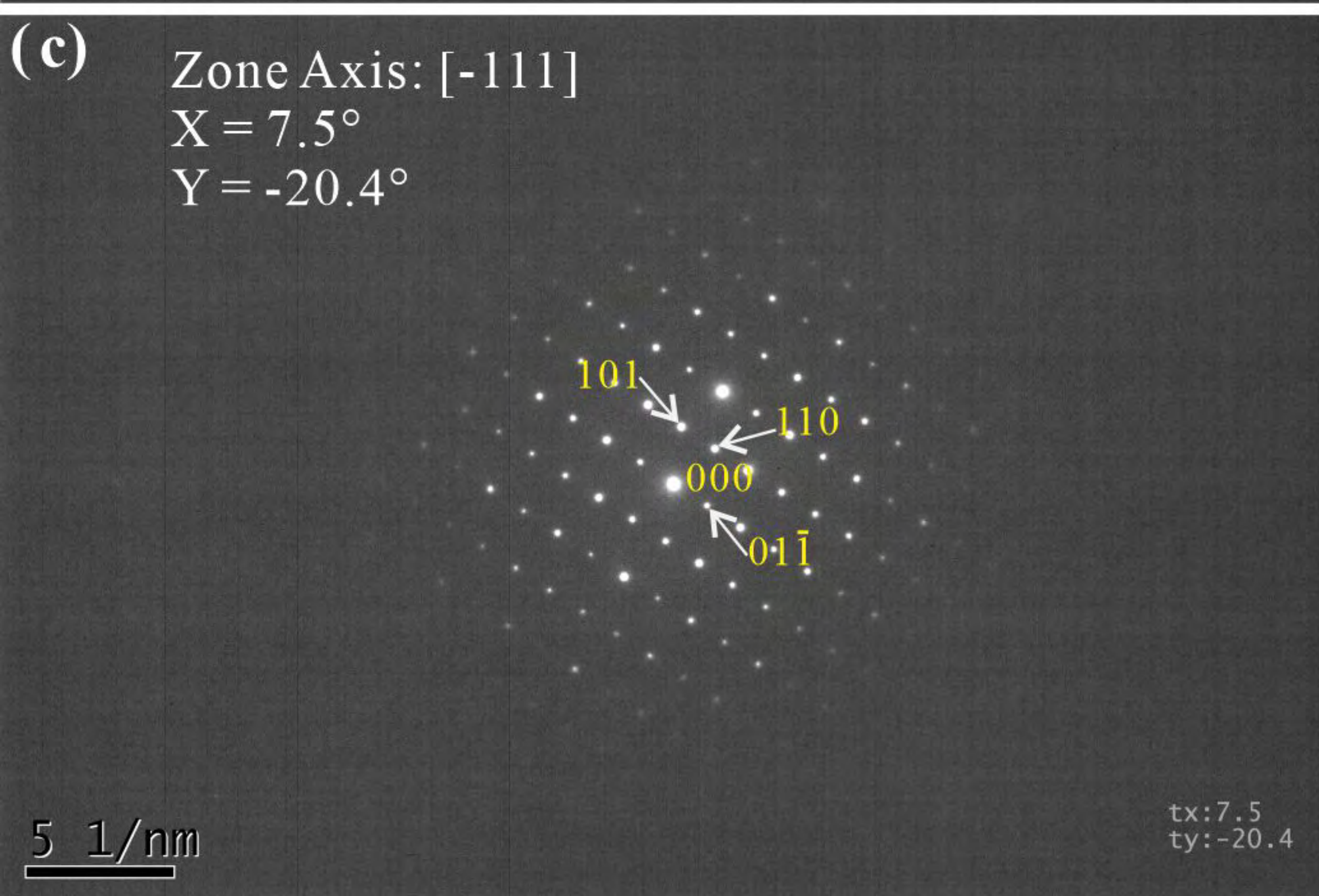
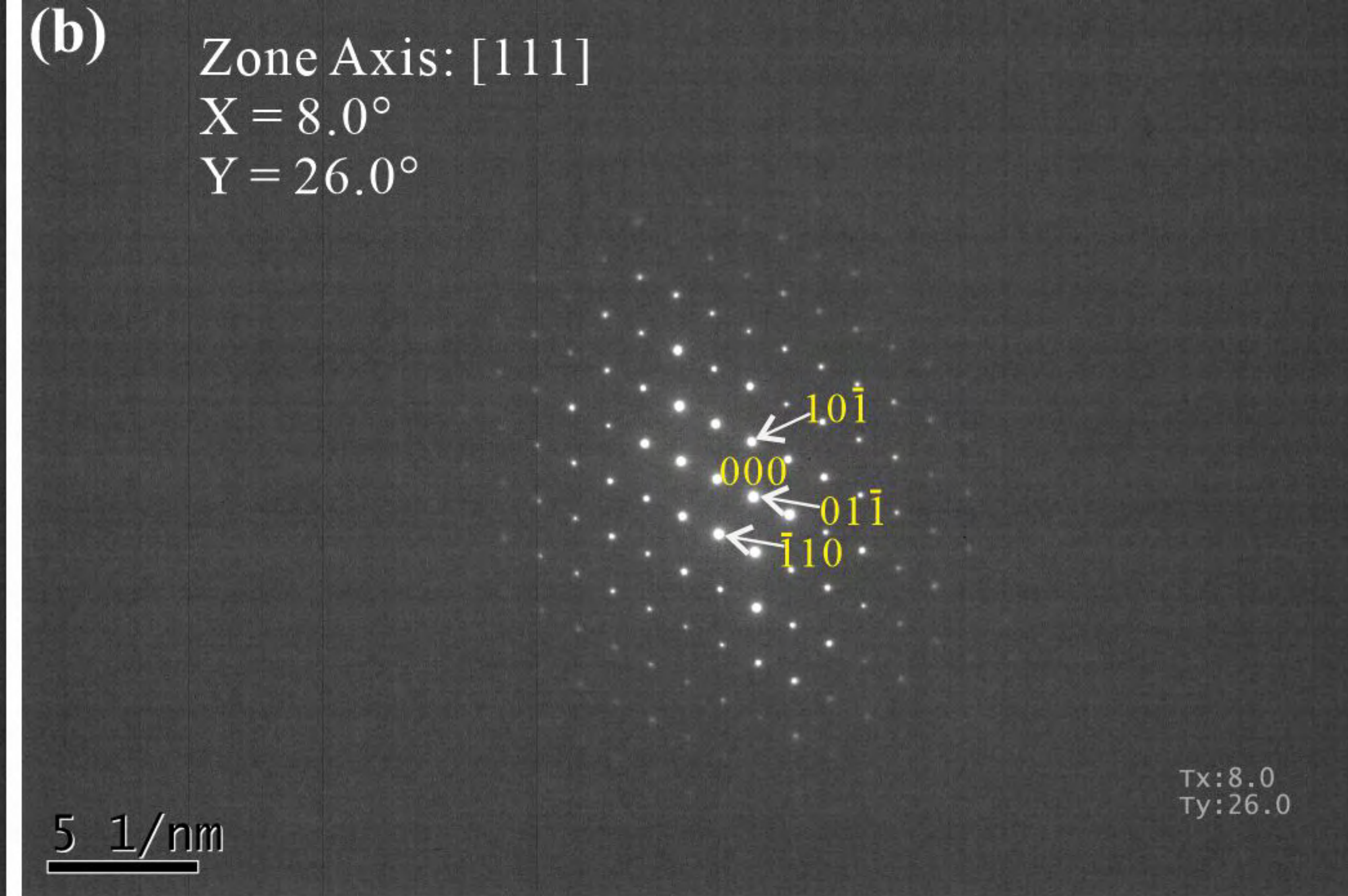
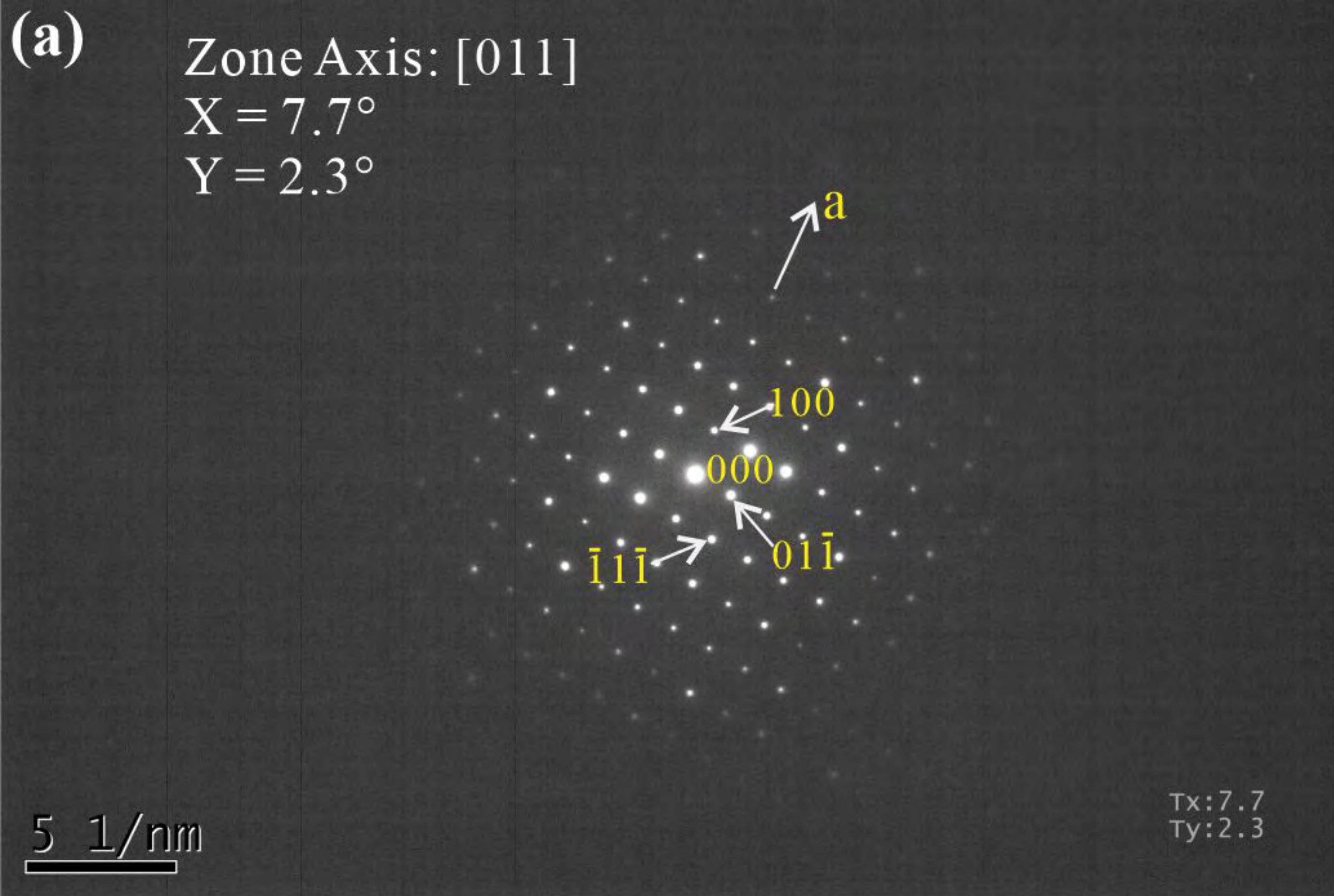


Fig. 7 revision 2



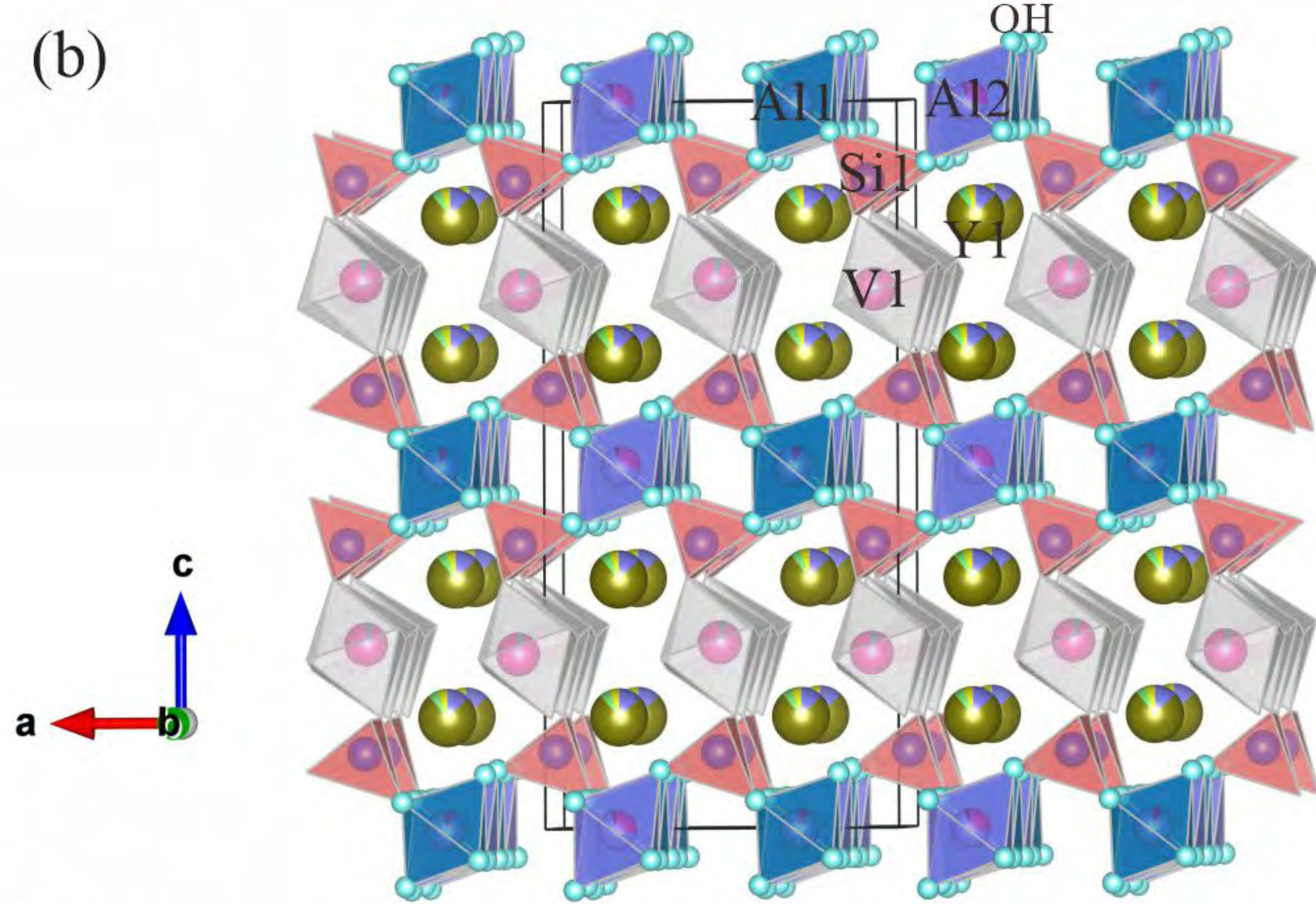
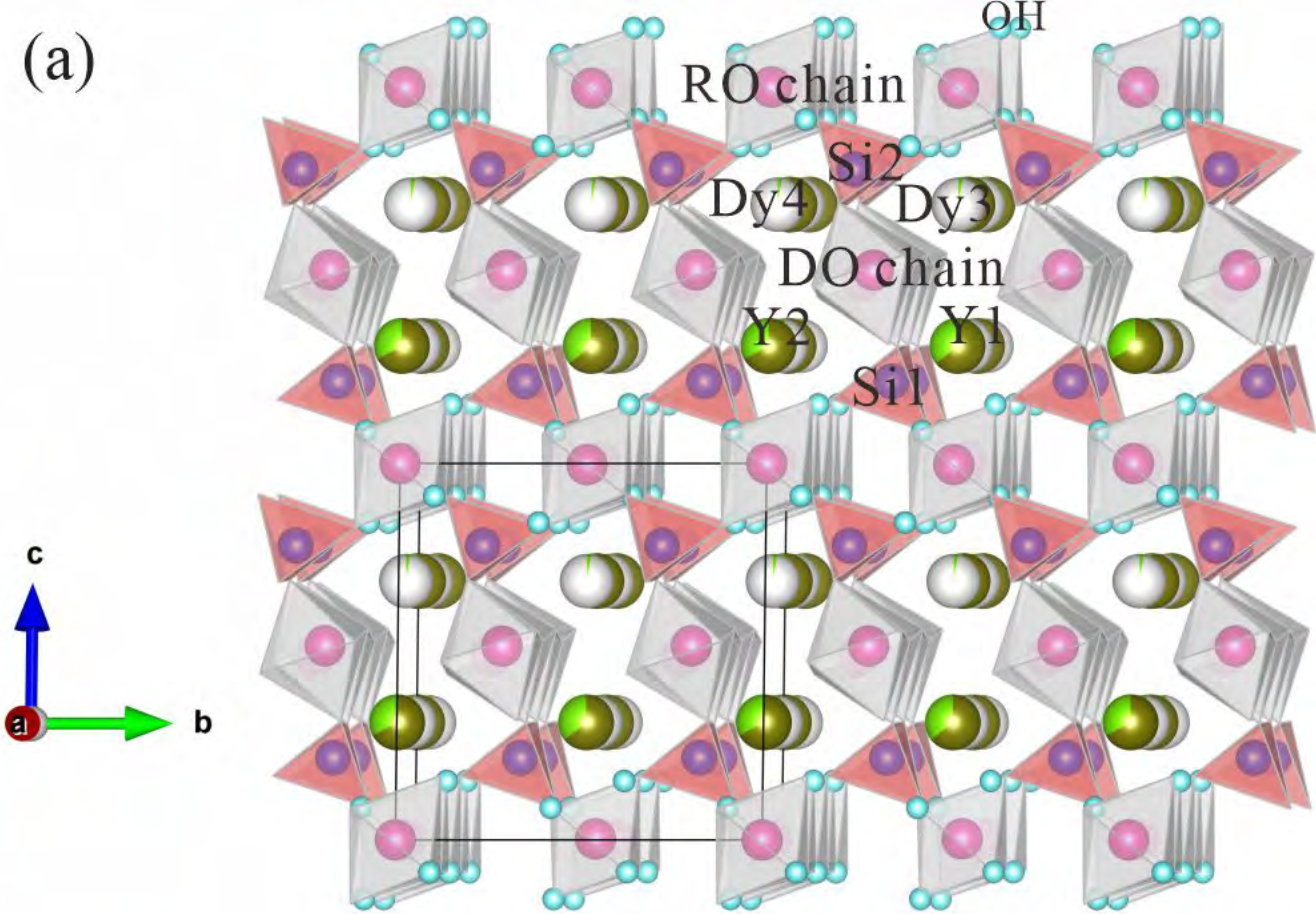


Fig. 8 revision 2

**Table 1.** Reflectance data for wenlanzhangite-(Y).

$\lambda$ (nm)	$R_{\max}$ (%)	$R_{\min}$ (%)
400	11.7	11.5
420	12.2	12.0
440	12.5	12.4
460	12.6	12.5
<b>470</b>	<b>12.7</b>	<b>12.5</b>
480	12.8	12.6
500	12.8	12.6
520	12.8	12.7
540	12.9	12.8
<b>546</b>	<b>12.9</b>	<b>12.8</b>
560	13.0	12.8
580	13.0	12.8
<b>589</b>	<b>13.0</b>	<b>12.9</b>
600	12.9	12.8
620	12.9	12.7
640	13.0	12.7
<b>650</b>	<b>13.0</b>	<b>12.7</b>
660	13.0	12.7
680	13.0	12.7
700	13.2	12.7

**Table 2.** Major-element data for wenlanzhangite-(Y) compared with jingwenite-(Y) (wt.%). Number of point analyses = 10.

Constituent	Jw-Y	Wlz-Y-1	-2	-3	-4	-5	-6	-7	-8	-9	-10	Mean (Wlz-Y)
SiO <sub>2</sub>	16.45	16.48	16.25	16.24	16.10	16.07	16.61	16.63	16.38	16.50	16.55	16.38
Al <sub>2</sub> O <sub>3</sub>	10.85	3.53	3.71	3.38	3.67	3.45	4.18	3.96	3.80	3.89	3.69	3.73
VO <sub>2</sub> *	21.65	22.25	22.40	22.28	22.10	22.05	22.55	22.60	22.49	22.49	22.40	22.36
V <sub>2</sub> O <sub>3</sub> *	4.04	14.96	15.17	15.42	14.81	14.90	14.07	14.49	15.04	14.27	14.51	14.76
Fe <sub>2</sub> O <sub>3</sub>	0.89	<mdl	<mdl	<mdl	<mdl	<mdl	<mdl	<mdl	<mdl	<mdl	<mdl	<mdl
TiO <sub>2</sub>	1.83	<mdl	<mdl	<mdl	<mdl	<mdl	<mdl	<mdl	<mdl	<mdl	<mdl	<mdl
Sc <sub>2</sub> O <sub>3</sub>	<mdl	0.34	0.20	0.19	0.21	0.15	0.66	0.62	0.21	0.65	0.46	0.37
Y <sub>2</sub> O <sub>3</sub>	24.67	18.55	19.12	19.13	19.04	18.92	19.30	19.55	19.45	19.59	19.26	19.19
Ce <sub>2</sub> O <sub>3</sub>	<mdl	0.50	0.33	0.39	0.26	0.42	0.33	0.38	0.35	0.31	0.36	0.36
Pr <sub>2</sub> O <sub>3</sub>	<mdl	0.14	0.17	0.08	0.20	0.19	0.13	0.23	0.12	0.28	0.19	0.17
Nd <sub>2</sub> O <sub>3</sub>	0.03	2.19	1.97	1.91	1.98	2.08	1.86	2.11	2.10	2.00	2.27	2.05
Sm <sub>2</sub> O <sub>3</sub>	0.1	1.38	1.27	1.21	1.26	1.16	1.40	1.51	1.26	1.41	1.48	1.33
Gd <sub>2</sub> O <sub>3</sub>	0.69	2.20	1.96	1.96	1.95	1.93	2.22	2.27	1.88	2.34	2.25	2.09
Tb <sub>2</sub> O <sub>3</sub>	0.32	0.45	0.59	0.51	0.59	0.67	0.58	0.49	0.63	0.49	0.57	0.56
Dy <sub>2</sub> O <sub>3</sub>	3.25	4.35	4.29	4.40	4.07	4.25	4.12	3.97	4.46	3.93	4.17	4.20
Ho <sub>2</sub> O <sub>3</sub>	0.83	0.61	0.71	0.67	0.85	1.11	0.68	0.54	0.54	0.83	0.67	0.72
Er <sub>2</sub> O <sub>3</sub>	3.55	2.80	3.08	3.03	3.02	3.11	2.61	2.42	3.03	2.60	2.55	2.83
Tm <sub>2</sub> O <sub>3</sub>	0.6	0.80	0.61	0.71	0.56	0.50	0.78	0.66	0.38	0.71	0.71	0.64
Yb <sub>2</sub> O <sub>3</sub>	3.99	2.24	2.74	2.70	2.60	2.55	2.34	2.18	2.60	2.20	2.22	2.44
Lu <sub>2</sub> O <sub>3</sub>	2.4	<mdl	<mdl	<mdl	<mdl	<mdl	<mdl	<mdl	<mdl	<mdl	<mdl	<mdl
H <sub>2</sub> O*	4.65	4.83	4.87	4.84	4.80	4.79	4.90	4.91	4.89	4.89	4.87	4.86
Total	101.23	98.58	99.43	99.04	98.05	98.32	99.33	99.51	99.59	99.37	99.19	99.04
	apfu	Calculated on basis of 8 cations										
Sc	-	0.04	0.02	0.02	0.02	0.02	0.07	0.07	0.02	0.07	0.05	0.04
Y	1.54	1.22	1.25	1.26	1.27	1.26	1.26	1.27	1.27	1.28	1.26	1.26
Ce	-	0.02	0.01	0.02	0.01	0.02	0.01	0.02	0.02	0.01	0.02	0.02
Pr	-	0.01	0.01	0.00	0.01	0.01	0.01	0.01	0.01	0.01	0.01	0.01
Nd	0.00	0.10	0.09	0.08	0.09	0.09	0.08	0.09	0.09	0.09	0.10	0.09
Sm	0.00	0.06	0.05	0.05	0.05	0.05	0.06	0.06	0.05	0.06	0.06	0.06
Gd	0.02	0.09	0.08	0.08	0.08	0.08	0.09	0.09	0.08	0.10	0.09	0.09
Tb	0.02	0.02	0.02	0.02	0.02	0.03	0.02	0.02	0.03	0.02	0.02	0.02
Dy	0.12	0.17	0.17	0.18	0.16	0.17	0.16	0.16	0.18	0.16	0.17	0.17

Ho	0.04	0.02	0.03	0.03	0.03	0.04	0.03	0.02	0.02	0.03	0.03	0.03
Er	0.14	0.11	0.12	0.12	0.12	0.12	0.10	0.09	0.12	0.10	0.10	0.11
Tm	0.02	0.03	0.02	0.03	0.02	0.02	0.03	0.03	0.01	0.03	0.03	0.02
Yb	0.14	0.08	0.10	0.10	0.10	0.10	0.09	0.08	0.10	0.08	0.08	0.09
Lu	0.08	-	-	-	-	-	-	-	-	-	-	-
Total (Sc,Y,REE)	2.13	1.98	1.99	1.99	1.99	2.01	2.01	2.01	1.99	2.04	2.02	2.00
Al	1.5	0.52	0.54	0.49	0.54	0.51	0.60	0.57	0.55	0.56	0.54	0.54
V <sup>3+</sup>	0.38	1.49	1.50	1.53	1.48	1.50	1.38	1.42	1.48	1.40	1.43	1.46
Fe	0.08	-	-	-	-	-	-	-	-	-	-	-
Total (Al,V,Fe) <sup>3+</sup>	1.96	2.01	2.04	2.02	2.02	2.00	1.98	1.99	2.03	1.97	1.97	2.00
V <sup>4+</sup>	1.84	2	2	2	2	2	2	2	2	2	2	2.00
Ti	0.16	-	-	-	-	-	-	-	-	-	-	-
Total (V,Ti) <sup>4+</sup>	2	2	2	2	2	2	2	2	2	2	2	2.00
Si	2	2.02	1.98	1.98	1.98	1.98	2.01	2.00	1.98	2.00	2.01	2.00
V <sup>3+</sup> /(V+Fe+Al) <sup>3+</sup>	0.19	0.74	0.74	0.76	0.73	0.75	0.70	0.71	0.73	0.71	0.73	0.73
Y/(REE+Y+Sc)	0.72	0.62	0.63	0.63	0.63	0.63	0.63	0.63	0.64	0.63	0.63	0.63

\*The VO<sub>2</sub> and V<sub>2</sub>O<sub>3</sub> contents were calculated based on the basis that V<sup>4+</sup> is ideally 2 apfu.

\*\*The H<sub>2</sub>O content was calculated on the basis of stoichiometry (i.e., OH = 4 apfu).

<mdl means below the minimum detection limit. Data for jingwenite-(Y) (Jw-Y) from Liu et al. (2023).

**Table 3.** Information on crystal and structural refinement for wenlanzhangite-(Y).

Crystal data	
Ideal chemical formula	$\text{Y}_2\text{V}^{3+}_2\text{V}^{4+}_2(\text{SiO}_4)_2\text{O}_4(\text{OH})_4$
Crystal size/mm	$0.02 \times 0.01 \times 0.005$
Crystal system	Triclinic
Space group	$P-1$ (#2)
Unit cell dimensions	$a = 5.9632(7) \text{ \AA}$
	$b = 9.5990(10) \text{ \AA}$
	$c = 9.9170(9) \text{ \AA}$
	$\alpha = 90.033(8)^\circ$
	$\beta = 98.595(9)^\circ$
	$\gamma = 90.003(9)^\circ$
Volume	$561.28(10) \text{ \AA}^3$
Z	2
Density (calculated)	$4.54 \text{ g/cm}^3$
Data collection and refinement	
Instrument	Rigaku-Oxford diffraction XtaLAB PRO-007HF
Radiation, wavelength, temperature	$\text{MoK}\alpha$ , 0.71073, 293(2) K
$2\theta$ range ( $^\circ$ )	5.938 to 58.414
$\mu / \text{mm}^{-1}$	14.448
$F(000)$	676
Total reflections	6438
Unique ref (all)	2583
Unique ref [ $I \geq 2\sigma(I)$ ]	1998
$R_{\text{int}}$	0.0494
$R_\sigma$	0.0587
Range of $h, k, l$	$-8 \leq h \leq 8; -12 \leq k \leq 13; -12 \leq l \leq 13$
$R_1, wR_2$ [ $I \geq 2\sigma(I)$ ]	$R_1 = 0.0736, wR_2 = 0.1813$
$R_1, wR_2$ [all data]	$R_1 = 0.0944, wR_2 = 0.1949$
Goodness-of-fit	1.090
No. of parameters, restraints	244, 19
Max./min. residual peak ( $\text{e \AA}^{-3}$ )	5.51/-2.90

**Table 4.** Site, Wyckoff position (*W.p.*), site occupancy (s.o.), fractional atomic coordinates and equivalent isotropic (and anisotropic) displacement parameters ( $\text{\AA}^2$ ) for wenlanzhangite-(Y).

Sites	<i>W.p.</i>	<i>x</i>	<i>y</i>	<i>z</i>	s.o.	$U_{\text{eq}}$
Y1	2i	0.56987(12)	0.49227(8)	0.31186(8)	0.70(2)Y+0.312(15)Dy	0.0127(3)
Y2	2i	-0.16344(13)	-0.00777(9)	0.31188(8)	0.74(2)Y+0.273(15)Dy	0.0135(3)
Dy3	2i	0.092(4)	0.492(2)	0.312(2)	0.021(3)	0.009(9)
Dy4	2i	0.678(4)	0.004(3)	0.690(3)	0.026(4)	0.028(9)
V1	2i	0.3986(3)	0.2206(2)	0.4849(2)	0.84(3)V+0.16(3)Al	0.0145(7)
V2	2i	0.9063(3)	0.2786(2)	0.5143(2)	0.82(3)V+0.18(3)Al	0.0145(8)
V3	2i	-0.2457(3)	0.4960(2)	-0.0029(2)	0.83(3)V+0.17(3)Al	0.0154(8)
V4	1a	1	0	1	0.93(4)V+0.07(4)Al	0.0110(9)
V5	1d	0.5	0	1	0.52(3)V+0.48(4)Al	0.0134(12)
Si1	2i	0.0503(5)	0.2859(3)	0.2177(3)	1	0.0144(8)
Si2	2i	0.6914(5)	0.2111(3)	0.7817(3)	1	0.0135(8)
O1	2i	0.4475(12)	0.1776(8)	0.6845(8)	1	0.0136(16)
O2	2i	-0.1465(11)	0.3203(8)	0.3151(8)	1	0.0153(17)
O3	2i	0.0317(13)	0.1216(8)	0.1701(8)	1	0.0145(16)
O4	2i	0.6976(13)	0.3761(8)	0.8303(9)	1	0.0194(18)
O5	2i	0.8992(12)	0.1828(8)	0.6919(8)	1	0.0139(16)
O6	2i	0.3007(11)	0.3136(8)	0.3097(8)	1	0.0157(17)
O7	2i	0.7286(12)	0.1098(9)	0.9162(8)	1	0.0163(17)
O8	2i	0.0206(12)	0.3882(8)	0.0814(8)	1	0.0155(17)
O9	2i	0.1051(12)	0.1231(9)	0.4738(9)	1	0.0191(18)
O10	2i	1.1332(14)	0.3827(9)	0.5582(9)	1	0.0220(19)
O11	2i	0.6172(13)	0.3729(8)	0.5260(8)	1	0.0160(17)
O12	2i	0.6048(14)	0.1151(9)	0.4396(9)	1	0.0217(18)
O13	2i	-0.4808(12)	0.3955(8)	0.0855(8)	1	0.0157(17)
O14	2i	0.2327(12)	0.1065(9)	0.9144(8)	1	0.0152(17)
O15	2i	0.5490(13)	0.1142(9)	1.1570(9)	1	0.0212(19)
O16	2i	-0.2182(12)	0.6092(9)	0.1566(9)	1	0.0185(18)

Sites	$U^{11}$	$U^{22}$	$U^{33}$	$U^{23}$	$U^{13}$	$U^{12}$
Y1	0.0129(5)	0.0203(5)	0.0056(4)	-0.0012(3)	0.0037(3)	-0.0011(3)
Y2	0.0139(5)	0.0216(6)	0.0067(5)	-0.0009(3)	0.0069(3)	-0.0014(3)
V1	0.0137(11)	0.0251(14)	0.0053(10)	0.0018(8)	0.0033(7)	-0.0057(8)
V2	0.0142(11)	0.0251(14)	0.0059(11)	0.0031(8)	0.0069(7)	0.0062(8)
V3	0.0118(12)	0.0276(16)	0.0077(13)	-0.0001(10)	0.0049(8)	-0.0020(8)
V4	0.0111(14)	0.0174(17)	0.0056(14)	0.0001(10)	0.0046(9)	0.0001(10)
V5	0.0121(18)	0.019(2)	0.0106(19)	0.0021(14)	0.0061(12)	0.0005(12)
Si1	0.0125(15)	0.0213(17)	0.0106(15)	-0.0026(12)	0.0055(11)	-0.0016(12)
Si2	0.0139(15)	0.0213(17)	0.0063(14)	0.0004(12)	0.0050(11)	0.0000(12)
O1	0.015(3)	0.021(4)	0.006(3)	-0.002(3)	0.007(3)	-0.004(3)
O2	0.007(3)	0.028(5)	0.011(4)	0.004(3)	0.006(3)	0.001(3)
O3	0.026(4)	0.014(4)	0.005(4)	0.002(3)	0.006(3)	-0.001(3)

O4	0.026(4)	0.017(4)	0.015(4)	0.003(3)	0.004(3)	0.005(3)
O5	0.020(4)	0.018(4)	0.006(3)	-0.003(3)	0.007(3)	-0.001(3)
O6	0.009(3)	0.029(5)	0.009(4)	0.000(3)	0.004(3)	0.002(3)
O7	0.017(4)	0.027(5)	0.006(4)	-0.001(3)	0.004(3)	0.000(3)
O8	0.012(3)	0.021(4)	0.015(4)	-0.002(3)	0.006(3)	-0.001(3)
O9	0.019(4)	0.021(4)	0.018(4)	0.008(4)	0.005(3)	0.000(3)
O10	0.028(4)	0.026(5)	0.011(4)	0.003(3)	0.000(3)	-0.004(3)
O11	0.025(4)	0.017(4)	0.007(4)	0.001(3)	0.006(3)	0.001(3)
O12	0.027(4)	0.027(5)	0.013(4)	-0.001(3)	0.011(3)	0.002(3)
O13	0.013(3)	0.019(4)	0.016(4)	-0.003(3)	0.004(3)	-0.001(3)
O14	0.012(3)	0.028(5)	0.007(4)	-0.001(3)	0.006(3)	0.002(3)
O15	0.019(4)	0.034(5)	0.011(4)	-0.007(4)	0.003(3)	-0.005(3)
O16	0.017(4)	0.029(5)	0.012(4)	-0.008(3)	0.010(3)	0.001(3)

---

**Table 5.** Selected bond lengths (Å) for wenlanzhangite-(Y).

Y1 Dy1–O2 <sup>1</sup>	2.360(7)	Y2 Dy2–O1 <sup>4</sup>	2.355(7)	Dy3–O2	2.18(2)
Y1 Dy1–O4 <sup>2</sup>	2.336(8)	Y2 Dy2–O3	2.316(7)	Dy3–O4 <sup>2</sup>	2.39(2)
Y1 Dy1–O6	2.347(8)	Y2 Dy2–O5 <sup>5</sup>	2.308(7)	Dy3–O6	2.12(2)
Y1 Dy1–O10 <sup>3</sup>	2.357(8)	Y2 Dy2–O9 <sup>4</sup>	2.376(8)	Dy3–O8	2.47(2)
Y1 Dy1–O11 <sup>2</sup>	2.457(8)	Y2 Dy2–O9	2.439(8)	Dy3–O10 <sup>2</sup>	2.33(2)
Y1 Dy1–O11	2.392(8)	Y2 Dy2–O12 <sup>6</sup>	2.330(8)	Dy3–O10 <sup>6</sup>	2.63(2)
Y1 Dy1–O13 <sup>1</sup>	2.406(8)	Y2 Dy2–O14 <sup>4</sup>	2.413(8)	Dy3–O11 <sup>2</sup>	2.54(2)
Y1 Dy1–O16 <sup>1</sup>	2.411(8)	Y2 Dy2–O15 <sup>7</sup>	2.426(9)	Dy3–O16	2.49(2)
<b>&lt;Y1 Dy1–O&gt;</b>	<b>2.383</b>	<b>&lt;Y2 Dy2–O&gt;</b>	<b>2.370</b>	<b>&lt;Dy3–O&gt;</b>	<b>2.39</b>
Dy4–O1	2.15(2)	V1 Al1–O1	2.001(8)	V2 Al2–O2 <sup>1</sup>	1.994(8)
Dy4–O3 <sup>5</sup>	2.38(3)	V1 Al1–O6	1.963(8)	V2 Al2–O5	1.993(8)
Dy4–O5	2.16(3)	V1 Al1–O9	1.973(8)	V2 Al2–O9 <sup>1</sup>	1.984(8)
Dy4–O7	2.44(3)	V1 Al1–O10 <sup>6</sup>	2.407(9)	V2 Al2–O10	1.686(9)
Dy4–O9 <sup>5</sup>	2.53(3)	V1 Al1–O11	1.961(8)	V2 Al2–O11	1.966(8)
Dy4–O12	2.67(3)	V1 Al1–O12	1.704(9)	V2 Al2–O12	2.418(9)
Dy4–O12 <sup>5</sup>	2.27(3)	<b>&lt;V1 Al1–O&gt;</b>	<b>2.002</b>	<b>&lt;V2 Al2–O&gt;</b>	<b>2.007</b>
Dy4–O15 <sup>8</sup>	2.46(3)				
<b>&lt;Dy4–O&gt;</b>	<b>2.38</b>				
V3 Al3–O4 <sup>7</sup>	2.001(9)	V4 Al4–O3 <sup>5</sup>	2.036(8)	V5 Al5–O7 <sup>8</sup>	2.000(8)
V3 Al3–O8	1.974(8)	V4 Al4–O3 <sup>11</sup>	2.036(8)	V5 Al5–O7	2.000(8)
V3 Al3–O8 <sup>9</sup>	1.989(8)	V4 Al4–O7	2.005(7)	V5 Al5–O14 <sup>8</sup>	1.976(7)
V3 Al3–O13	2.009(8)	V4 Al4–O7 <sup>12</sup>	2.005(7)	V5 Al5–O14	1.976(7)
V3 Al3–O13 <sup>10</sup>	2.004(7)	V4 Al4–O14 <sup>8</sup>	2.011(8)	V5 Al5–O15	1.890(8)
V3 Al3–O16	1.906(8)	V4 Al4–O14 <sup>1</sup>	2.011(8)	V5 Al5–O15 <sup>8</sup>	1.890(8)
<b>&lt;V3 Al3–O&gt;</b>	<b>1.981</b>	<b>&lt;V4 Al4–O&gt;</b>	<b>2.017</b>	<b>&lt;V5 Al5–O&gt;</b>	<b>1.955</b>
Si1–O2	1.661(8)	Si2–O1	1.652(8)		
Si1–O3	1.645(8)	Si2–O4	1.654(9)		
Si1–O6	1.651(8)	Si2–O5	1.653(8)		
Si1–O8	1.659(9)	Si2–O7	1.639(8)		
<b>&lt;Si1–O&gt;</b>	<b>1.654</b>	<b>&lt;Si2–O&gt;</b>	<b>1.650</b>		

Symmetry codes: (i) 1+X,+Y,+Z; (ii) 1-X,1-Y,1-Z; (iii) 2-X,1-Y,1-Z; (iv) -X,-Y,1-Z; (v) 1-X,-Y,1-Z; (vi) -1+X,+Y,+Z;

(vii) -1+X,+Y,-1+Z; (viii) 1-X,-Y,2-Z; (ix) -X,1-Y,-Z; (x) -1-X,1-Y,-Z; (xi) 1+X,+Y,1+Z; (xii) 2-X,-Y,2-Z



**Table 6.** Comparison between wenlanzhangite-(Y) and jingwenite-(Y)

	Jingwenite-(Y)	Wenlanzhangite-(Y)
Ideal Formula	$\text{Y}_2\text{Al}_2\text{V}^{4+}_2(\text{SiO}_4)\text{O}_4(\text{OH})_4$	$\text{Y}_2\text{V}^{3+}_2\text{V}^{4+}_2(\text{SiO}_4)_2\text{O}_4(\text{OH})_4$
Z	4	2
Crystal System	Monoclinic	Triclinic
Space Group	$I2/a$ (#15)	$P-1$ (#2)
$\text{V}^{3+}/(\text{V}^{3+}+\text{Al}+\text{Fe}^{3+})$	0.19	0.58-0.72 (mean = 0.67)
Unit-cell parameters	$a = 9.4821(2)\text{Å}$	$a = 5.9632(7)\text{Å}$
	$b = 5.8781(1)\text{Å}$	$b = 9.599(1)\text{Å}$
	$c = 19.3987(4)\text{Å}$	$c = 9.9170(9)\text{Å}$
	$\beta = 90.165(2)^\circ$	$\alpha = 90.033(8)^\circ$
	$V = 1081.21(4)\text{Å}^3$	$\beta = 98.595(9)^\circ$
		$\gamma = 90.003(9)^\circ$
		$V = 561.28(10)\text{Å}^3$
Reference	Liu <i>et al.</i> (2023)	This study